Aggregation-Dependent Epitope Sequence and Modification Fingerprints of Anti-Aβ Antibodies

Talucci Ivan[1, 2]; Leske Timon[1]; Klafki Hans-Wolfgang[3]; Hassan Mohammed Mehedi[3]; Steiert Annik[3]; Morgado Barbara.[3]; Bothe Sebastian[1]; van Werven Lars[4]; Liepold Thomas[4]; Walter Jochen[5]; Schindelin Hermann[1]; Wiltfang Jens[3]; Wirths Oliver[3]; Jahn Olaf[3,4]; Maric Hans-Michael[1]

Author affiliations:
[1] Rudolf Virchow Center for Integrative and Translational Bioimaging, Julius-Maximilians-Universität (JMU) Würzburg, Germany
[2] Department of Neurology, University Hospital Wuerzburg (UKW), Würzburg, Germany
[3] Department of Psychiatry and Psychotherapy, University Medical Center Göttingen (UMG), Germany
[4] Neuroproteomics Group, Department of Molecular Neurobiology, Max Planck Institute for Multidisciplinary Sciences, Göttingen, Germany
[5]Center of Neurology, Molecular Cell Biology, University Hospital Bonn, Germany
Correspondence to H.M.M. at hans.maric@uni-wuerzburg.de

Abstract

A hallmark of Alzheimer's disease (AD), the most common form of dementia, is the progressive accumulation of amyloid-beta (Aβ) peptides across distinct brain regions. Anti-Aβ antibodies (Aβ-Abs) targeting specific Aβ variants are essential tools for AD research, diagnostics, and therapy. The monoclonal antibodies Aducanumab, Lecanemab, and Donanemab have recently been approved as the first disease-modifying treatments for early AD, highlighting the clinical importance of their exact binding profiles.

In this study, we systematically characterized the binding and modification requirements of 20 Aβ-Abs, including biosimilars of Aducanumab, Lecanemab, and Donanemab, across monomeric, oligomeric, and aggregated Aβ forms. Array-based analysis of 20,000 modified Aβ peptides defined binding epitopes at single-residue resolution and revealed the impact of sequence variation, including familial AD mutations, as well as diverse post-translational modifications (PTMs). Notably, genetic variants such as H6R impaired binding of therapeutic Aβ-Abs like Aducanumab. Donanemab showed strong preference for pyroglutamate-modified AβpE3–10, while Lecanemab and Aducanumab exhibited aggregation- and sequence-context-dependent binding requirements.

Comparison of peptide binding profiles with binding of full-length and aggregated Aβ via immunoprecipitation-mass spectrometry, capillary immunoassays, Western blotting, and immunohistochemistry on AD brain tissue revealed distinct aggregation-dependent binding behaviours. The valency- and context-dependence of Aducanumab binding, together with its preference for Ser8-phosphorylated Aβ, supports a dimerization-mediated binding mechanism. For Lecanemab, our data suggest that additional structural contributions beyond the minimal N-terminal epitope are required for binding to aggregated Aβ, which remain to be fully resolved.

Together, this work provides the most comprehensive dataset to date on aggregation-dependent sequence and modification selectivity of Aβ-Abs. By integrating mutational, PTM, and aggregation contexts in a unified experimental framework, we establish a resource that enables rational selection of antibodies for research and diagnostic applications, and offers mechanistic insights that may inform the design and optimization of future therapeutic antibodies in AD.

Introduction

Alzheimer's disease (AD) is a neurodegenerative disorder characterized by the accumulation of amyloid-beta (Aβ) [1,2] and tau tangles in the brain, leading to cognitive decline and dementia [3]. Aβ peptides are generated under physiological conditions from Amyloid Precursor Protein (APP) by sequential proteolytic cleavages by beta- and gamma-secretase [4]. The initial β-secretase cleavage of APP results in the release of soluble sAPPβ and the generation of a 99 amino acids (AA) long carboxy (C)-terminal APP fragment (C99) with an amino (N)-terminal Asp-residue. Aβ peptides are generated by subsequent gamma-secretase cleavage of C99 [5,6].

In human cerebrospinal fluid, a conserved pattern of soluble Aβ1-37, Aβ1-38, Aβ1-39, Aβ1-40 and Aβ1-42 has been observed [7]. Aβ peptides isolated from amyloid plaques have been shown to include several variants differing in length, their N- and C-termini, and post-translational modifications (PTMs) [8], such as cyclization of N-terminal Glu(3) or Glu(11) into pyroglutamate (pE) [9], and racemization or isomerization of Asp(1) and Asp(7) [10-13]. Furthermore, phosphorylated forms of Aβ (pSer(8) and pSer(26)) have been reported in amyloid plaques based on studies employing phospho-selective anti-Aβ antibodies (Aβ-Abs), although these findings have not yet been conclusively confirmed by mass spectrometry [14-16]. In extracellular senile plaques in the brain's functional tissue, the parenchyma, Aβ1-42 is more prevalent than Aβ1-40, and various N- and C-terminally truncated [17-20] as well as N-terminally elongated variants [21] have been described [5,22]. In particular, those starting with a cyclized pE (3) [12] or Phe at position 4 [21,23], are highly abundant in AD brains [24]. Genetic mutations [25] further multiply Aβ amino acid sequence variability. The study of the structural polymorphisms of the Aβ peptide resulting from PTMs or mutations and the potential impact on the formation of pathophysiological oligomeric forms and fibrillar aggregates is challenging [26-30]. The majority of PTMs occur in the flexible N-terminal region of the fibrils, encompassing residues 1–16, and were proposed to trigger or accelerate the fibrillation of Aβ [31-33]. The same region is responsible for metal ion coordination which may also influence fibril formation [34]. Similarly, several pathogenic APP mutations within Aβ are associated with altered folds, higher aggregation propensities, and toxicities [35-37].

Importantly, this complexity requires molecular tools with appropriate molecular specificity and sensitivity and poses enormous challenges in designing sensitive diagnostic readouts and effective targeted therapies. Passive immunotherapy using monoclonal Aβ-Abs has been investigated extensively as an approach for AD treatment resulting in Aβ-Abs with several

different Aβ selectivity profiles [38] [39]. For example, Aducanumab, a recombinant human antibody, was developed after screening human memory B-cells for reactivity towards aggregated Aβ [40,41]. Bapineuzumab, the humanized form of the murine antibody 3D6 [42] has been reported to bind to both monomeric and aggregated Aβ.

Despite extensive structural, genetic, and pre-clinical investigations, clinical trials of Aβ antibodies have yielded ambiguous outcomes. Aβ antibody binding to cerebral amyloid angiopathy (CAA) has been hypothesized to correlate with the frequency of amyloid-related imaging abnormalities with edema (ARIA-E) observed in patients treated with Aβ-based immunotherapies [38]. Aducanumab, developed by Neurimmune AG and later licensed to Biogen. was investigated in two parallel Phase 3 clinical trials: EMERGE demonstrated statistically significantly slower decline in the Clinical Dementia Rating Sum of Boxes for a high dose of Aducanumab vs. placebo, while ENGAGE failed to meet its primary endpoints [43]. Marketing and development of Aducanumab was halted in 2024 [44]. Lecanemab was designed at Uppsala University, humanized by BioArctic, and later licensed to Eisai. It showed positive results in the Clarity AD trial, and, cross-study comparison suggested that Lecanemab [45,46] has lower ARIA-E frequency than Aducanumab (13% vs 25-35%) [38], Lecanemab is now marketed as Leqembi. Eli Lilly's Donanemab, approved in the US as Kisunla, binds to CAA fibrils in proportion to the amount of pyroglutamate-modified Aβ they present [38] [47]. These divergent outcomes highlight the importance of thoroughly characterizing each antibody's epitope specificity, binding affinity for Aβ variants, ability to access relevant brain compartments, and possible genetic confounders (such as APOE ε4).

Aβ-Abs are the primary means for the detection and targeting of specific Aβ variants within the outlined Aβ-sequence and -modification space. The precise molecular binding epitopes of Aβ-Abs are fundamental to Aβ research. However, the immunogens used to raise and select Aβ-Abs may not represent precise and reliable predictors of the actual sequence and modification requirements. Furthermore, epitope requirements reported by different mapping methodologies may differ and may thus render a comparison difficult. Here we addressed the range and limitations of the sequence and modification specificity by side-by-side comparison in complementary assays for a panel of 20 Aβ-Abs central to AD research and therapy.

Results and Discussion

The Aβ-Abs investigated in this study are listed in **Table 1**. The panel encompasses biosimilars of the currently FDA-approved drugs (i) Aducanumab (Biogen), initially approved for the treatment of mild cognitive impairment [44] but discontinued in 2024 (ii) Lecanemab (Biogen, Uppsala University and Eisai) [48], which in contrast to Aducanumab, has been approved via regular approval track and (iii) Donanemab (Eli Lilly) as the most recent expansion of the AD-drug arsenal [49,50]. The set of Aβ-Abs further encompasses selected antibodies directed against specific Aβ variants such as Aβ1-x with a free N-terminal-Asp(1) (3D6, 82E1, 11H3, 80C2), N-truncated Aβ starting with pE(3) (AβpE3-x) (pE3-Aβ, 2-48 and $Donanemab_{bs}$) and phosphorylated Aβ forms (1E4E11, 5H11C10). Furthermore, the panel covers Aβ-Abs against the N-terminal region of Aβ and a central epitope, as well as antibodies selective for N-terminally elongated and truncated Aβ variants.

Antibody[a]	*Source*[b]	*Clonality*[c]	*Species*[d]	*Immunogen*[e]	*Mod.*[f]	*Array*[g]	*Refs.*
3D6	Creative Biolabs (#PABL-011)	Mono	Mouse	1-5	-	1-5	[42,51-53]
pAb77	Dept. of Psych., Göttingen	Poly	Rabbit	2-14	-	3-16	[54]
4G8	Biolegend (#800701)	Mono	Mouse	17-24	-	17-21	[21,55]
11H3	Nanotools (#bA4N-11H3)	Mono	Mouse	1-x	-	1-4	-
82E1	IBL (#10323)	Mono	Mouse	1-16	-	1-4	[53,56]
14-2-4	IBL	Mono	Mouse	(-3)-5	-	(-2)-3	[21]
7H3D6	Center of Neurol., Bonn	Mono	Rat	1-14	-	1-10	[57]
1E4E11	Abcam (#ab219817)	Mono	Mouse	p1-14	pSer8	3-8	[57]
5H11C10	Center of Neurol., Bonn	Mono	Mouse	p20-34	pSer26	19-32	[14]
pAb58-1	Dept. of Psych., Göttingen	Poly	Rabbit	4-9	-	4-9	[56]
Aβ-pE3	Synaptic Systems (#218003)	Poly	Rabbit	pGlu3-7	pE3	3-7	[58]
80C2	Synaptic Systems (#218231)	Mono	Mouse	1-5	-	1-5	[53]
2-48	Synaptic Systems (#218011)	Momo	Mouse	pGlu3-7	pE3	3-7	[59]
101-1-1	Dept. of Psych. Göttingen	Mono	Mouse	(−3)-5	-	(-2)-3	[21,60]
IC16	Dept. of Neuropath. Düsseldorf	Mono	Mouse	1-16	-	1-8	[61-63]
6E10	Covance (#SIG-39320)	Mono	Mouse	1-16	-	3-8	[55,60]
1E8	Nanotools (#bA4N-1E8)	Mono	Mouse	1-x	-	3-8	[52]
$Aducanumab_{bs}$	Proteogenix (#PX-TA1335)	Mono	Human	-	-	1-7	[41]
$Donanemab_{bs}$	Proteogenix (#PX-TA1549)	Mono	Humanized	pGlu3-42	pE3	3-10	[47,64]
$Lecanemab_{bs}$	Proteogenix (#PX-TA1746) and BioXCell (#BXC-SIM0032)	Mono	Humanized	1-42	-	3-7	[48]

Table 1 – Footnotes: (a) names of the anti-amyloid beta antibodies. (b) Source of the antibodies used in this study, either commercial or academic. (c) Clonality of the antibodies:

"mono" indicates monoclonal, while "poly" stands for polyclonal antibodies. (d) Species of origin for the IgGs: mouse, rat, human, or rabbit. (e) Immunogens, as reported in the literature, that were used to generate the corresponding antibodies. (f) If available, the anticipated PTM specificity is indicated: “p” represents phosphoserine (at positions Ser8 or Ser26), and “pE3” refers to an N-terminal pyroglutamate (at position 3). (g) epitope identified in this study on microarrays.

Pre-screening of Aβ-Ab Epitopes

Information regarding binding epitopes and /or immunogens for most of the tested Aβ-Abs has been published and is summarized in **Table 1**. However, the binding epitope information was derived from varying methodologies. To provide an initial side-by-side comparison we pre-screened all of the listed Aβ-Abs in array format using copies of peptide libraries and standard antibody concentrations of 0.5-1 µg/mL (**Figure 1a)**. The library comprised the amyloid precursor protein (APP770) residues 649-722, corresponding to the canonical Aβ1-42 amino acid sequence with additional 23 amino terminal and 9 carboxy terminal residues. To enable single amino acid resolution, 60 peptides with a length of 15AA and overlapping by 14AA were synthesized and displayed as cellulose-conjugates incapable of oligomerization (**Figure 1b**). We first focused on Aβ-Abs with known preference for Aβ starting with a free Asp(1) and initially found that 3D6 and 82E1 also detected Aβ(2-x) and several N-terminally elongated Aβ-related peptides in addition to Aβ(1-x), at least under the generic pre-screening conditions with presumably suboptimal Ab concentrations (**Figure 1b**). Thus, it is clear that antibodies must be titrated for each specific application to obtain selectivity and to reduce non-specific binding. For optimal signal to noise ratios and ideal selectivity profiles on the microarrays, the Aβ-Ab concentrations were adjusted for 3D6, 82E1, 11H3, 80C2 and 7H3D6 (**Figure 1 – figure- supplement 1**) and (**Appendix 1-7**). This setup allowed to determine the general location of the binding epitopes within the Aβ sequence for all tested Aβ-Abs as shown by the heatmap in (**Figure 1b).** Similarly, Donanemab [47,64], 1E4E11 [57], and 5H11C10 [14], which have been previously reported as selective for AβpE3, pSer8Aβ, and pSer26-Aβ, respectively, produced detectable signals in this pre-screening with unmodified Aβ-related peptides. Again, these findings demonstrate the need for further investigation to confirm selectivity under more appropriate assay conditions, i.e. optimized antibody concentrations and presentation of modified Aβ-fragments as binding partners. The side-by-side determined epitopes are summarized together with their immunogen in **Table 1.** Epitope mapping recapitulated previously reported data, but also further confines (pAb77, 4G8, 14-2-4, 101-1-1, 6E10, 1E8, 7H3D6, 1E4E11, 5H11C10) or even expands (Aducanumab$_{bs}$) the required

154 residues for binding. However, although this initial microarray only contained unmodified Aβ
155 sequences, we also observed binding for Aβ-Abs known as PTM-selective. Specifically,
156 Donanemab$_{bs}$, 2-48 and Aβ-pE3 were raised against AβpE3-x (**Table 1**) and were expected to
157 show preference for Aβ peptides starting with a pE(3). In the pre-screening with unmodified
158 Aβ sequences, however, Donanemab$_{bs}$ detected Aβ(3-x) starting with non-cyclized Glu (3),
159 Aβ(-3-x) as well as several other N-terminally elongated Aβ-related peptides and Aβ1-x. Since
160 the primary binding mode for AβpE3-x had not yet been tested at this stage these initial
161 screening observations remain preliminary. Similarly, 1E4E11 and 5H11C10, which were
162 reported to have high selectivity for phosphorylated Aβ peptides at Ser8 and Ser26 [14,57],
163 both displayed strong signals with several non-phosphorylated Aβ variants in the pre-
164 screening. Although the findings with the modification-selective Aβ-Abs are indicative of
165 cross-reactivity due to the presence of epitopes resembling their target and/or the effect of
166 suboptimal binding conditions, the unbiased microarray screening provided valuable initial
167 information regarding the sequence regions and modifications of interest to be investigated in
168 more detail in the course of our study.

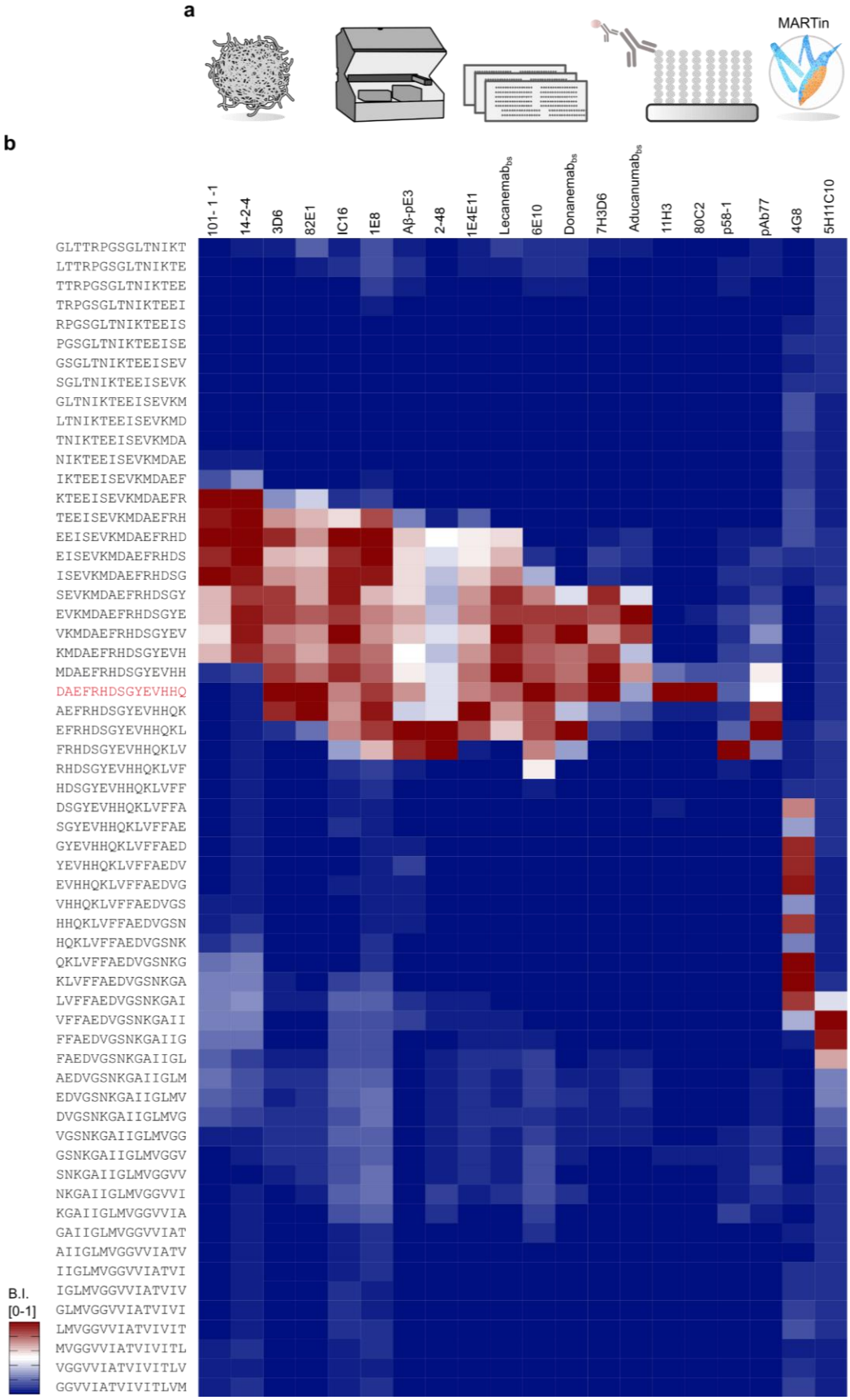

Figure 1. Microarray workflow and Aβ-Ab epitope pre-screening. (a) Schematic of the microarray workflow. The library comprised the amyloid precursor protein (APP) residues 649-722 (APP770 numbering), corresponding to Aβ residues -23 to 51, as a library of 15-mer

173 peptides overlapping by 14AAs, copied in dozens, and probed for Aβ-Abs binding followed
174 by analysis in MARTin. (b) The epitope screening binding data are summarized as a heatmap.
175 Blue and red shades indicate the relative binding strength of the related arrayed peptides to the
176 left and cognate Aβ-Ab on top. The blue – red scale is visualizing the normalized binding
177 intensity for each antibody individually. The applied antibody concentrations ranged between
178 0.5-1 µg/mL. Note: Among the 20 tested antibodies, 1E4E11, 5H11C10, 2-48, Aβ-pE3, and
179 $Donanemab_{bs}$ have known PTM-selectivity, which could not be fully addressed with the initial
180 microarray consisting of unmodified Aβ fragments only.

181 Titration and Selectivity Assessment of Aβ Abs Directed Against 182 the Aβ N-terminus

183 The sensitivity and selectivity profiles of Aβ-Abs 80C2, 11H3, 3D6, 82E1, which were
184 expected to show preferential binding to Aβ with a free N-terminal Asp(1), and mAb 7H3D6
185 were explored in more detail. The canonical Aβ peptide is typically 40-42 amino acids long. In
186 addition, various N-terminal variants have been reported [53]. Several truncated forms have
187 been detected in brain tissue [21,24]. Notably, N-terminally truncated Aβ peptides, particularly
188 those starting with Phe at position 4, are abundant in AD brains. The metalloproteinase
189 ADAMTS4, which is expressed in oligodendrocytes, has been linked to APP processing and
190 the generation of Aβ4-x peptides [23]. Additionally, N-terminally elongated Aβ peptides, such
191 as Aβ(-3-x), which can be generated by the same enzyme in cell culture [21], may be of interest
192 in the context of AD biomarker research: Aβ(-3-40) can serve as a reference in a composite
193 blood-based biomarker of AD for cerebral Aβ accumulation [65,66]. Highly sensitive and
194 selective Aβ-Abs for N-terminal Aβ variants are a prerequisite for studying their specific roles
195 in detail. In our microarray experiments, the titration of Aβ-Abs expected to prefer Aβ1-x
196 variants with a free N-terminal Asp (mAbs 80C2, 11H3, 3D6, 82E1) plus the rat monoclonal
197 7H3D6 (Figure 1 Supplement **1**) (**Appendix 1**) broadly classifies the tested mAbs into two
198 groups. One group (80C2 and 11H3) that, on microarray under the tested experimental
199 conditions, displayed exclusive binding towards Aβ1-x over the entire titration range albeit
200 with limited sensitivity. A second group showed high sensitivity but concentration-dependent
201 and limited Aβ1-x selectivity over related Aβ variants under the tested conditions (3D6, 82E1
202 and 7H3D6). Among the 20 tested antibodies, 1E4E11, 5H11C10, 2-48, Aβ-pE3, and
203 $Donanemab_{bs}$ exhibited the previously reported preferences for PTMs, which will be addressed
204 in detail in the following paragraphs.

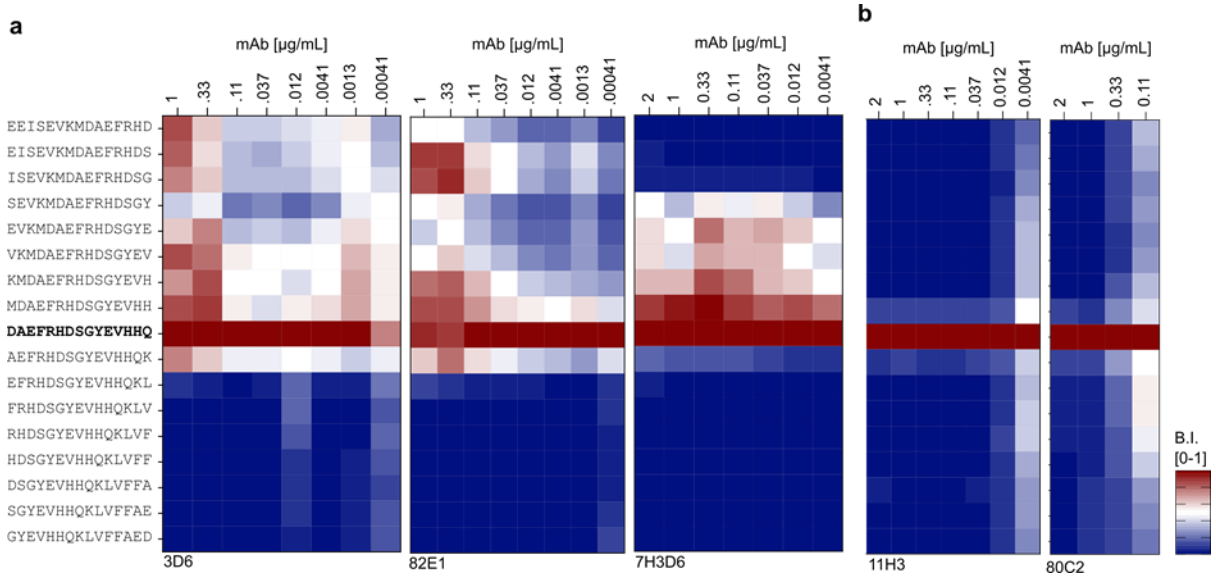

Figure 1 - figure supplement 1. Titration series of N-terminal specific Anti-Aβs. (a) Titration of monoclonal Aβ-Ab 3D6, 82E1 and 7H3D6 at concentrations ranging from 2 to 0.00041 µg/mL to study the selectivity for free-Asp(1) over Asp(1) within an N-terminal elongated peptide. The signals were normalized internally and presented as a heat map with blue-to-red shades ranging from 0 to 1. (b) Monoclonal Aβ-Ab 11H3D6 and 80C2 exhibited high selectivity towards free-Asp(1) across the chosen concentration range of 2 µg/mL down to 0.0041 µg/mL.

Deep Mutational Scans Provide Information on Aβ-Abs Binding Requirements

Next, we further explored the reactivities observed during the epitope pre-screening (**Figure 1**) and probed in total 14 selected monoclonal antibodies with matched deep mutational libraries. Apart from the biosimilar Abs and the Abs directed against the Aβ N-terminus described above, we also selected three generic Aβ Abs as references (IC16, 1E8, 6E10) and two Abs selective for N-terminally elongated Aβ variants (14-2-4, 101-1-1), the core epitope of which we have described earlier [21]. Display and binding evaluation of all possible point-mutants systematically resolved the sequence requirements for these 14 Aβ-Abs towards the binding region corresponding to the Aβ(-10-18) amino acid sequence (**Figure 2A - figure supplement 1**) in three different 18-meric positional scans. Peptides covering Aβ(-10-8) **(Figure 2b)**, Aβ(-3-15) **(Figure 2c)** and Aβ1-18 **(Figure 2d)** regions were generated. As these three peptide regions showed binding to most of the N-terminal antibodies (**Figure 1**), we postulated that these 18-mers should cover the main antigen-antibody (Ag/Ab) contact regions. The three Aβ-related wild-type sequences were sequentially scanned from N-terminus to C-terminus by replacing each position by every proteinogenic amino acid (342 different peptide

229 sequences in total). A customized criterion was utilized to identify the core motif for each
230 monoclonal antibody tested. While the identified core motifs are essential for binding, they
231 may not fully represent the specificity of the antibodies but rather indicate where the majority
232 of the Ag/Ab contact takes place. Specifically, the raw mean intensities for all peptide variants
233 were measured and normalized against the corresponding wildtype sequence. Amino acid
234 exchanges that reduced binding by >50% were designated as dominant negative. This process
235 was reiterated for each exchange at that position. Positions were considered as major
236 contributor to the core motif when more than 50% of the exchanges were marked as dominant
237 negative. The resulting core motifs are summarized in **Figure 2 – figure supplement 1D**. The
238 findings highlight both similarities and differences in the binding mode of different Aβ-Abs,
239 affirming binding to epitopes located in the N-terminal region of the Aβ sequence. Overall, this
240 comprehensive binding data provides guidance for sorting monoclonal Aβ-Abs based on
241 epitope properties. For two of the tested antibodies, namely 3D6 and Aducanumab, crystal
242 structures are publicly available [41] [42], and indicate binding in the regions Aβ1-5 (3D6) and
243 3-7 (Aducanumab), respectively. Here, the microarray results recapitulated the epitope of 3D6
244 (murine precursor of Bapineuzumab) and expanded the binding interface for Aducanumab$_{bs}$
245 binding to monomeric short Aβ fragments by two residues, namely Asp(1) and Ala(2) (**Figure
246 2D, Figure 2 - figure supplement 1A, B)**. Donanemab is known to recognize Aβ starting with
247 cyclized pE3 [47,64], however, on our initial microarray screen, Donanemab$_{bs}$ showed clear
248 signals with AβpE3-x and several other Aβ related peptides starting N-terminally of Glu(3),
249 including Aβ1-x (**Figure 1**). To further explore this unexpected observation, Donanemab$_{bs}$ was
250 tested on the Aβ (1-18) deep mutational scan. Consistent with its expected preference for the
251 Aβ3-x region, the primary Ag/Ab contacts for the binding to Aβ1-18 involved the amino acids
252 *EFRHDSGY.* Asp(1) and Ala(2) were not highly conserved. Importantly, the murine precursor
253 antibody mE8 from which Donanemab was derived was previously shown to have a very strong
254 preference for truncated AβpE3(starting with pyroglutamate) [64]. This particular point is
255 further addressed in detail in the paragraph "Modification selectivity of monoclonal Aβ-Abs
256 mAbs" (see below). The monoclonal Ab 1E4E11, which was previously reported to be highly
257 selective for phosphorylated pSer(8)-Aβ [57], bound to unphosphorylated Aβ2-16 and several
258 other unphosphorylated Aβ-related peptides on the initial screen (**Figure 1**). Interestingly, the
259 profiling of Ser(8) did not show elevated binding to the phospho-mimetic exchanges (Asp or
260 Glu) (**Figure 2D**). The effect of phosphorylation at Ser(8) is also addressed in detail in the
261 paragraph "Modification selectivity of monoclonal Aβ-Abs" mAbs (see below). As shown in
262 (**Figure 2 – figure supplement 2D**), several Aβ-Abs exhibited altered binding strength with

263 exchanges R5G or Y10F which may be valuable information when studying the co-aggregation
264 dynamics between exogenous (human) and endogenous (mouse) Aβ in transgenic models.

265 The data set presents the sequence requirements of 14 Aβ-Abs for binding to 18-mer Aβ-related
266 peptides in a microarray setup, thereby complementing previous structural insights and further
267 improving our understanding of their molecular mode of action.

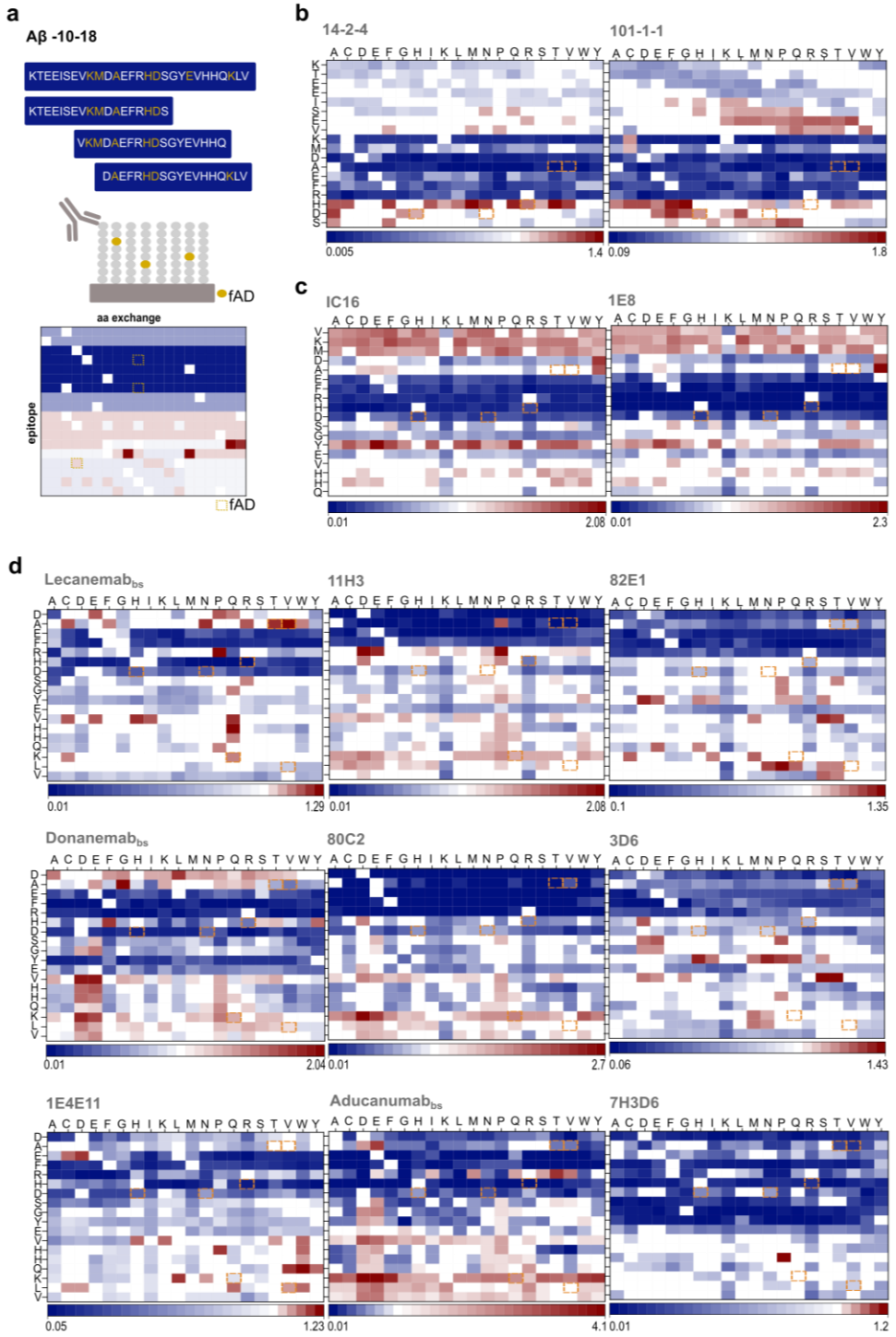

268

269 **Figure 2. Deep Mutational Scans Define Aβ-Ab Core Sequences** (a) Schematic summary of
270 the three deep positional scans in the N-terminal region. Seven reported APP mutations are

271 indicated as yellow boxes. From each 18-mer epitope, positional substitutions were generated
272 (342 variants for each epitope) and tested semi-quantitatively in microarray format. The wild-
273 type (wt) sequence was sequentially scanned from N to C terminal by turning each position
274 into every proteinogenic amino acid. Consequently, the contribution of each residue is depicted
275 in blue-white-red shades, with white corresponding to no variation from wt [1] and blue-to-red
276 representing loss or gain of binding strength. (b) Fingerprint analysis for the first peptide group
277 covering the sequence *KTEEISEVKMDAEFRHDS*. The Aβ-Abs tested here are *101-1-1* and
278 *14-2-4*. (c) Fingerprint analysis for the second peptide group covering the sequence
279 *VKMDAEFRHDSGYEVHHQ*. The Aβ-Abs tested here are IC16 and 1E8. (d) Fingerprint
280 analysis for the third peptide group covering the sequence *DAEFRHDSGYEVHHQKLV*. The
281 Aβ-Abs tested here are Aducanumab, Donanemab and Lecanemab biosimilars. In addition,
282 commercially available Aβ-Abs such as 3D6, 82E1, 11H3, 80C2, 7H3D6 and 1E4E11 were
283 included. Note: The antibodies, 1E4E11 and Donanemab$_{bs}$ have known reported PTM-
284 preference which will be addressed in the next paragraphs.

285 Hereditary APP Mutations Affect Antibody Binding

286 Next, we studied the impact of some reported hereditary mutations in the *APP* gene resulting
287 in amino acid exchanges within the Aβ sequence [25]. Specific familiar *APP* gene mutations
288 [25,67] are reported to either lead to aggressive forms of AD or to exert a protective effect.
289 Several mutations in the Aβ peptide have been reported to cause familial AD (fAD), with all
290 but two having a dominant pattern of inheritance [67,68]. These alterations can lead to
291 enhanced aggregation and increased cytotoxicity, contributing to the onset and progression of
292 early-onset AD. The following APP mutations within the Aβ amino acid sequence were
293 included in the microarray screen: D7H [69], D7N [70], H6R [71], A2V[72], A2T [73,74],
294 K16Q [75,76], L17V [77].

295 Our analysis indicates that genetic mutations causing amino acid exchanges in or close to the
296 Aβ sequence can affect antibody binding. Regarding the biosimilar antibodies Lecanemab$_{bs}$,
297 Donanemab$_{bs}$ and Aducanumab$_{bs}$, this may potentially have relevance for rare fAD and their
298 therapeutic implications. The APP mutants D7H/7N, H6R and A2T/V, K16Q and L17V are
299 highlighted in the deep mutational scan data (**Figure 2** and **Figure 2 – figure supplement 1**),
300 as they were identified within the core motifs of the Aβ-Abs. The mutations A2V, D7H, D7N,
301 and H6R can lead to an increased aggregation propensity of Aβ and contribute to early onset
302 fAD [78]. Specifically, D7H (Taiwan), D7N (Tottori), and H6R (English) mutations may alter
303 the structural features and thermodynamics of Aβ42, leading to increased β-sheet [79] content.
304 For confirmation and for highlighting the importance of considering genetic variability for
305 therapeutic responses, we next paradigmatically explored the effects of the D7H, D7N, H6R,

A2V and A2T APP mutations [71] on Aducanumab$_{bs}$ binding to short monomeric Aβ-related peptides on microarray.

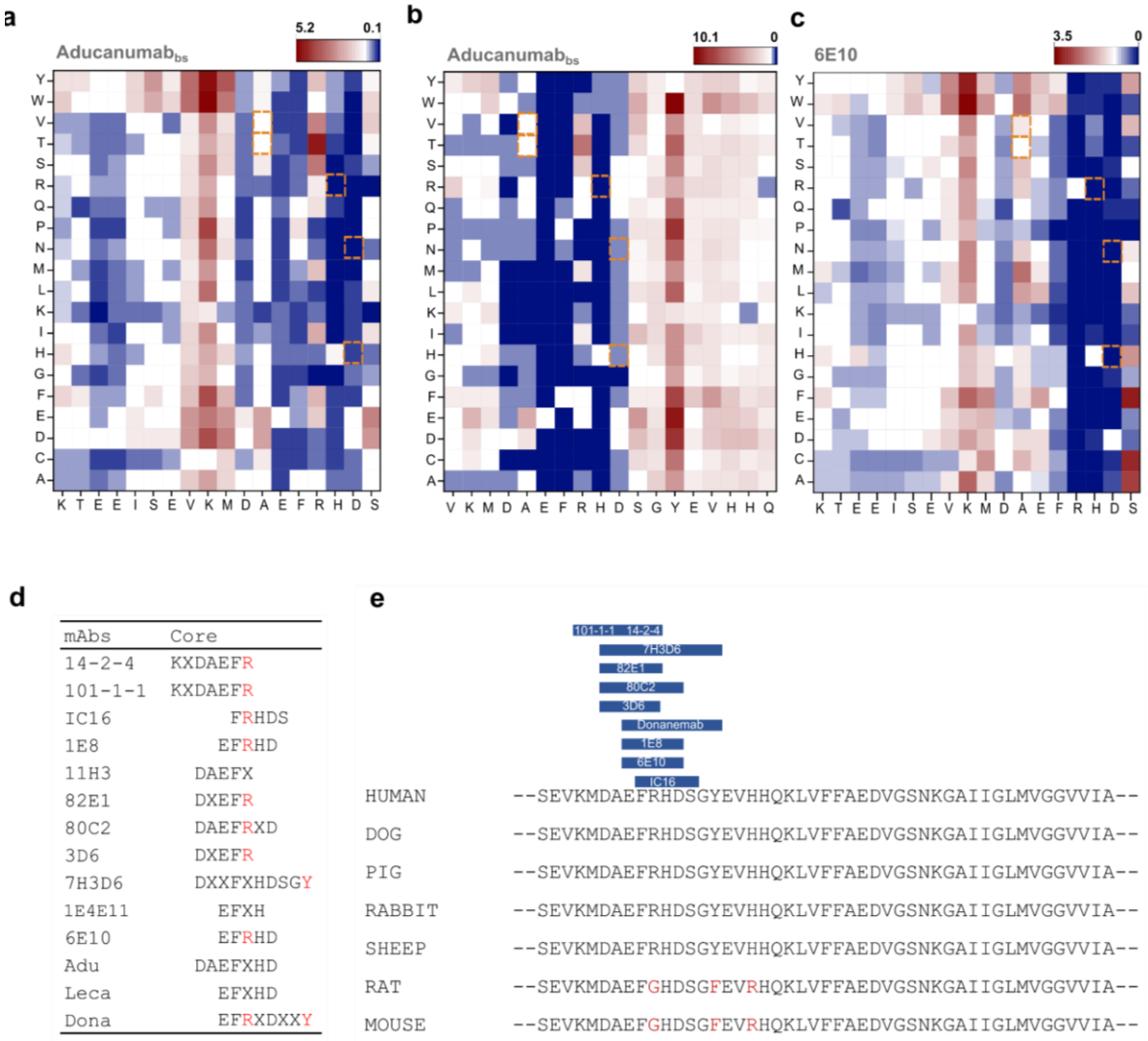

mAbs	Core
14-2-4	KXDAEFR
101-1-1	KXDAEFR
IC16	FRHDS
1E8	EFRHD
11H3	DAEFX
82E1	DXEFR
80C2	DAEFRXD
3D6	DXEFR
7H3D6	DXXFXHDSGY
1E4E11	EFXH
6E10	EFRHD
Adu	DAEFXHD
Leca	EFXHD
Dona	EFRXDXXY

Figure 2 - figure supplement 1. N-terminally elongated Deep Mutational Scans of Aducanumab$_{bs}$ and 6E10 with core motifs summary. (a) Fingerprint analysis for the first peptide group covering the sequence *KTEEISEVKMDAEFRHDS*. The Aβ-Ab tested here is Aducanumab$_{bs.}$ (b) Fingerprint analysis for the second peptide group covering the sequence *VKMDAEFRHDSGYEVHHQ*. The Aβ-Ab tested here is Aducanumab$_{bs.}$ (c) Fingerprint analysis of 6E10 on the sequence *KTEEISEVKMDAEFRHDS*. (d) Summary of the antibody core motifs, "X" within the sequence stands for non-conserved residue. When an amino acid variation led to a decrease in binding below 50% of wt, it was marked as dominant negative. If more than 10 amino acid substitutions were dominant negative, the entire position was designated as part of the core motif (represented in single-letter coding). (e) Aβ-Ab species preferences. Amino acid positions which are different in human and rat/mouse are highlighted in red. These specific positions were probed. Antibodies showing altered binding strength after replacing R5 or Y10 in the human Aβ sequence by G5 or F10 (rat/mouse Aβ sequence) are highlighted in blue. Human: Homo Sapiens; Dog: Canis Lupus Familiaris; Pig: Sus Scrofa; Rabbit: Oryctolagus Cuniculus; Sheep: Ovis Aries; Rat: Rattus Norvegicus; Mouse: Mus Musculus.

The Mutation H6R Abolishes Aducanumab Binding

Consistently across the two deep positional scans, Aducanumab$_{bs}$ and 6E10 showed significantly reduced binding intensity to 18-mer peptides on the array in case of the fAD H6R mutation [71]. This aligns closely with previous findings [55], which identified *RXD* as the minimal sequence required for 6E10 binding via phage mapping (present in 53% of immunoprecipitated sequences). Our data indicate that 6E10 exhibits binding to a broader motif, *EFRHD* and shows that H6 is necessary for binding. To confirm our findings and underscore the potential significance of genetic variability in possible therapeutic strategies, we subsequently measured the binding affinity of Aducanumab$_{bs}$ to Aβ(1-15, H6R) [71]. First, we spotted the corresponding purified peptides *DAEFR**H**DSGYEVHHQ* and *DAEFR**R**DSGYEVHHQ* (**Figure 2 – figure supplement 2a**) (**Appendix 8**) at 2-fold dilutions. The semi-quantitative on chip titration confirmed a reduced binding strength of Aducanumab$_{bs}$ for the H6R Aβ1-15 variant. For complete quantification including kinetic evaluation, we next conducted Biolayer Interferometry (BLI) experiments (**Figure 2 – figure supplement 2b**). The BLI response of Aducanumab$_{bs}$ for the H6R was completely abolished when compared with the wildtype sequence. These data confirm the array profiling and, in broader context, highlight a possible gap in efficacy for monoclonal Aβ-Abs in individuals with certain rare hereditary mutations associated with AD, which may have implications for personalized treatment approaches. However, whether or not the H6R amino acid replacement could impact also the binding of Aducanumab$_{bs}$ to aggregated Aβ is still unclear.

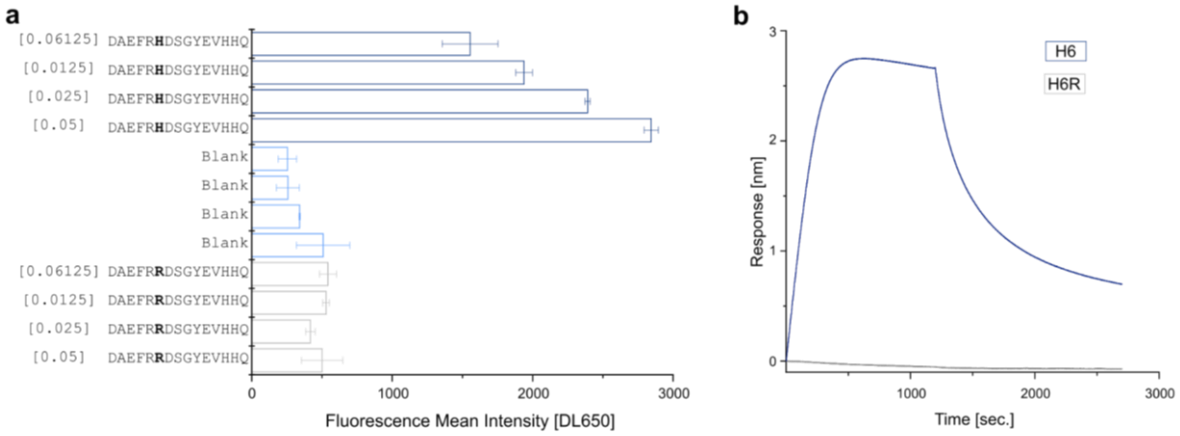

Figure 2 – figure supplement 2. Aβ1-15 carrying the English mutation (H6R) shows reduced affinity for Aducanumab$_{bs}$. (a) Dot Blot from the purified 6xHis peptides *DAEFR**H**DSGYEVHHQ* and *DAEFR**R**DSGYEVHHQ* were printed using Slide Spotter robot. IgG signals were detected using Goat anti-human DL650, in square brackets the µg/mL of

350 Aducanumab$_{bs.}$ (b) The Biolayer interferometry responses of Aducanumab$_{bs}$ (10nM) over the
351 NTA-loaded *DAEFR**H**DSGYEVHHQ* and *DAEFR**R**DSGYEVHHQ* peptides are shown.

352 Modification Selectivity of Monoclonal Aβ-Abs

353 PTMs of Aβ can significantly impact aggregation propensity [31], clearance mechanisms, and
354 toxicity in AD. Specific PTMs might be associated with different stages of AD progression and
355 severity, offering potential biomarkers for diagnosis and prognosis. Targeting PTMs represents
356 a potential therapeutic strategy to prevent Aβ aggregation and neurotoxicity, thereby slowing
357 disease progression. *In vitro*, Aβ cyclization of N-terminal Glu into pE, and
358 racemization/isomerization of Asp were shown to increase the aggregation propensity and
359 neurotoxicity [12,80]. Therefore, a selected group of PTM-carrying Aβ peptides (PTM-Aβ)
360 were incorporated into the Aβ chip to explore the potential binding preference of selected Aβ-
361 Abs, under optimized concentrations (**Figure 3**). The antibodies were tested with both PTM-
362 Aβ and the corresponding unmodified variants to provide a head-to-head comparison. This
363 screening was performed in the presence of Aβ phosphorylated at positions Ser(8) or Ser(26),
364 N-terminal pE at position 3, racemization/isomerization of Asp at position 1, and unmodified
365 N-terminal variants. The dataset is divided into sections (**Figure 3 a-f**) for enhanced
366 visualization, where each antibody was screened simultaneously against all peptides to locate
367 their epitope preferences. Post-hoc mass spectrometry (MS) analysis validated the correct
368 display of the PTM variants included in the microarray (**Appendix 1-6**). A set of antibodies
369 without reported PTM preference was applied here as controls (**refer to Table 1**), namely
370 11H3, 101-1-1, IC16, 82E1 and 3D6. Antibody 6E10 has been previously shown to be unable
371 to detect Aβ-pSer(8) and was thus also included as a control antibody [81]. On the microarray
372 and under the tested experimental conditions, Aducanumab$_{bs}$ and 1E4E11 (**Appendix 10**)
373 showed preference for Aβ peptide fragments phosphorylated at Ser(8) (pSer(8)). Donanemab$_{bs}$,
374 2-48, and Aβ-pE3 exhibited high selectivity for Aβ peptides starting with an N-terminal pE
375 (**Figure 3D**) over Aβ3-x starting with a non-cyclized Glu and other Aβ variants. In contrast,
376 mAb IC16 showed weaker binding to AβpE3-x than to Aβ3-x. Abs 7H3D6 and 11H3 did not
377 recognize Iso-Asp(1), while 11H3 interestingly showed no affinity for D-Asp(1)-modified Aβ
378 peptides. As expected, all of the tested antibodies, which are directed against the N-terminal
379 Aβ region, did not show appreciable binding, and only 5H11C10 bound to the phosphorylated
380 Ser(26) when the modification was localized centrally within Aβ19-32 (**Figure 3E, F**).

381

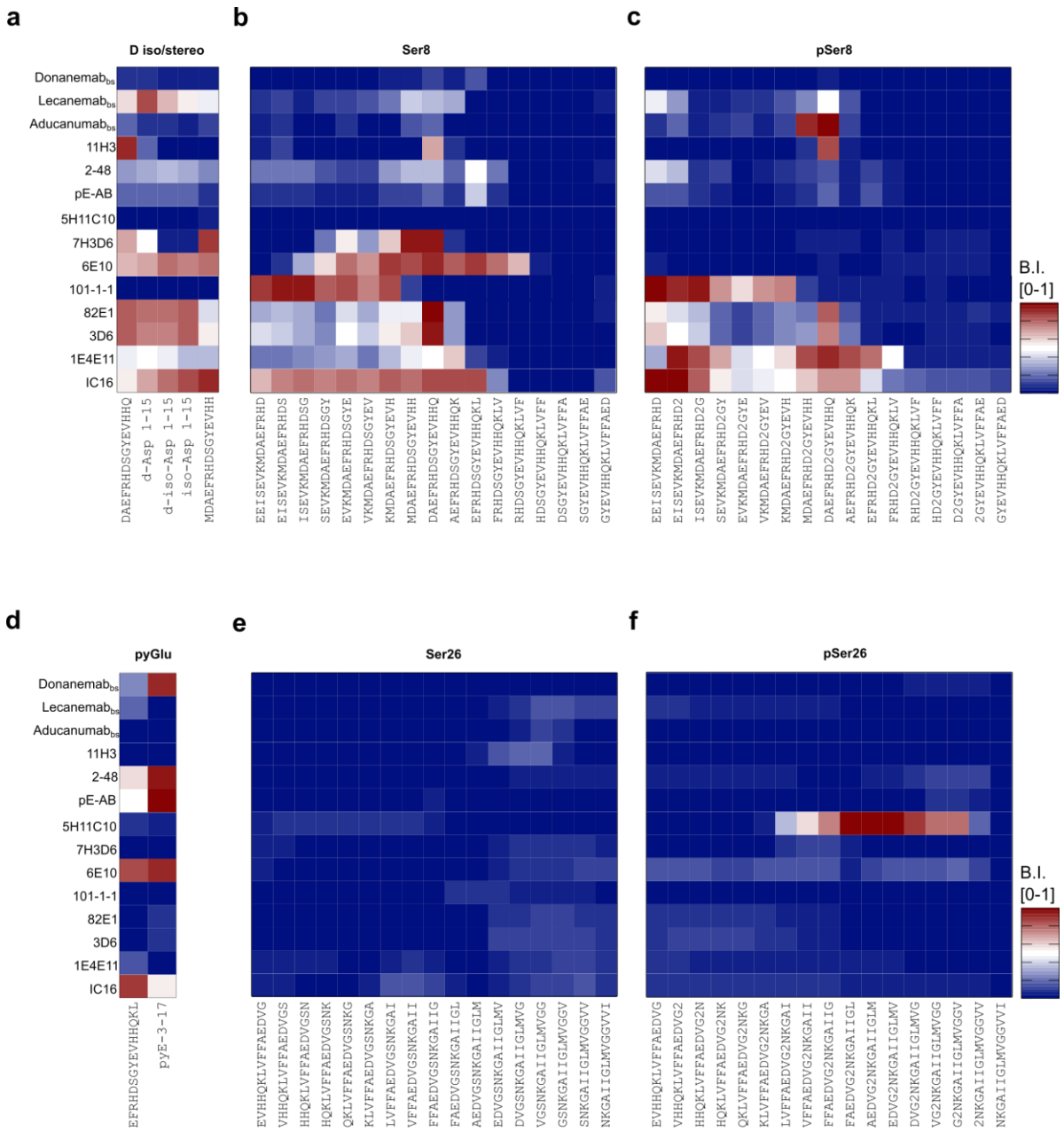

Figure 3. Multiplex Analysis of Aβ-Abs with preference for post-transcriptionally modified Aβ variants

The signals were normalized internally and presented as a heat map ranging from 0 to 1. Blue and red shades indicate the binding strength over the related arrayed post-transcriptionally modified peptide shown on top and cognate anti-Aβ antibody to the left. The antibodies were tested under optimal dilutions: 6E10, IC16, Aβ-pE3, 1E411, 101-1-1, 5H11C10, 2-48 at 0.25µg/mL; Lecanemab$_{bs}$, Donanemab$_{bs}$ at 0,0012µg/mL; Aducanumab$_{bs}$ at 0.02µg/mL; 3D6, 11H3, 82E1 at 0.037 µg/mL; 7H3D6 at 0.012µg/mL. The dataset is split over different sections (a-f) to allow proper visualization. Each antibody was screened in parallel against all modifications. (a) The control peptide Aβ(-1-14) was used alongside Asp(1) isomers and stereoisomers. (b) The region overlapping with unmodified Serine 8. (c) The region overlapping with modified phospho Serine 8 (represented as '2'). (d)Tthe control unmodified

395 3-17 was used alongside pE3. (e) The region overlapping with unmodified Serine 26. (f) The
396 region overlapping with modified phospho Serine 26 (represented as '2').

397 pSer8-Preference of Aducanumab$_{bs}$ in the Context of Non-
398 Aggregated Aβ

399 Aducanumab has been reported to preferentially target aggregated Aβ [40] and bind
400 monomeric Aβ with low micromolar affinity [41], tetrameric Aβ1-15 with low nanomolar
401 affinity and aggregated Aβ with sub-nanomolar affinity corresponding to a roughly 10.000-
402 fold enhanced affinity for Aβ aggregates [40,41]. However, in our hands, on microarray and
403 under the tested experimental conditions, we observed appreciable binding of Aducanumab$_{bs}$
404 to short, monomeric Aβ-related peptides (**Figures 1, 2, 3**), which we followed up by studying
405 some molecular details. Prompted by the observed preference of Aducanumab$_{bs}$ for
406 phosphorylated pSer8-Aβ(-1-14) and pSer8-Aβ1-15 over unphosphorylated Aβ-related 15-
407 mers on our microarrays (**Figure 3,Figure 3 - supplement 2A**), we sought to quantify the
408 underlying relative affinity differences using the purified epitope variants in BLI as a proof-of-
409 concept experiment with the caveat that the assay may affect the absolute affinity due to
410 multivalency and high-density effects. As a reference, mAb 1E4E11 was titrated over the
411 immobilized phosphorylated Aβ variant (**Figure 3, figure supplement 1**) (**Appendix 9**). As
412 expected, mAb 1E4E11 showed a strong response in the nanomolar affinity range with fast on
413 rates and very slow off rates, resulting in a K_D of 4 nM**.** In contrast, the overall response was
414 at least within an order of magnitude lower with the unphosphorylated peptide and showed fast
415 off rates, resulting in a quantified K_D of only 1.3μM for mAb1E4E11 binding. Overall, mAb
416 1E4E11 showed a 300-fold preference for the phosphorylated Aβ variant in this assay.

417 Henceforth, we applied this methodology to Aducanumab$_{bs}$ (**Figure 3 – figure supplement 2**)
418 and observed a preference for monomeric Aβ1-15 phosphorylated at Ser(8) over
419 unphosphorylated Aβ1-15. Initially, both modified and unmodified Aβ1-15 peptides were
420 loaded onto the BLI sensors and tested with different antibody concentrations. The affinity for
421 the phosphorylated variant was at least 6 times higher than for the unmodified peptide,
422 however, on microarray, the EC50 for the pSer8-Aβ1-15 was 300 times lower than that for the
423 corresponding unphosphorylated peptide (**Appendix 10**). Importantly, this was only detectable
424 on semi-quantitative array analysis, which can be explained by multivalency effects that may
425 lower the observed antibody off-rate. Overall, the affinity quantification in BLI did not result
426 in a large difference between the two variants and we thus concluded that Aducanumab$_{bs}$ has

427 agnostic preference for a negative charge, either provided by a carboxylic (Asp or Glu – see
428 **Figure 2**) or phosphoserine group (**Figure 3 – figure supplement 2**), as it was not selective
429 for the latter. This is in strong opposition to the state-of art pSer(8) antibody 1E4E11, which
430 did not recognize phoshomimetic amino acid exchanges such as aspartate or glutamate (**Figure**
431 **2**). This observation raised the question of whether Aducanumab$_{bs}$ is involved in electrostatic
432 interaction.

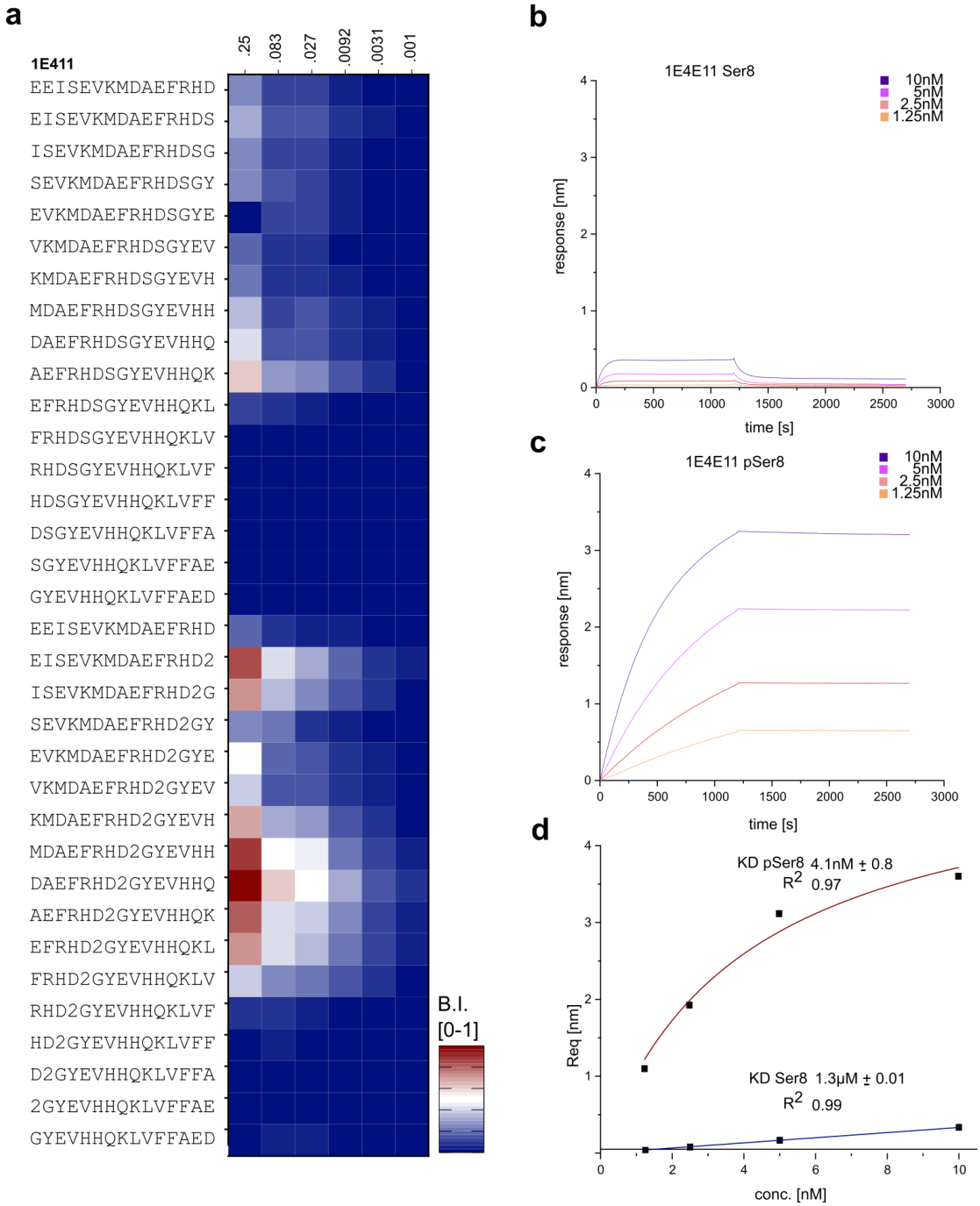

433

434 **Figure 3 – figure supplement 1. Antibody 1E4E11 shows high preference for**
435 **phosphorylated pSer8 Aβ1-15 in μSPOT and BLI assays.** (a) Titration of monoclonal Aβ-

436 Ab 1E4E11 at concentrations ranging from 0.25 to 0.001 µg/mL to achieve high selectivity for
437 Aβ1-15 phosphorylated at Ser(8). The modified pSer is represented as '2'. The signals were
438 globally normalized against *DAEFRHDpSGYEVHHQ* and presented as a heat map with blue-
439 to-red shades ranging from 0 to 1. (b) BLI dose-response curve of mAb 1E4E11 binding to the
440 NTA-loaded *DAEFRHDSGYEVHHQ-6xHis-amide* peptide. (c) Biolayer interferometry dose-
441 response curve of mAb 1E4E11 binding to the NTA-loaded *DAEFRHDpSGYEVHHQ-6xHis-*
442 *amide* peptide. (d) BLI steady-state analysis revealed K_Ds of 4.1nM and 1.3µM for Aβ1-15
443 with phosphorylated and unphosphorylated Ser (8), respectively (1:1 model).

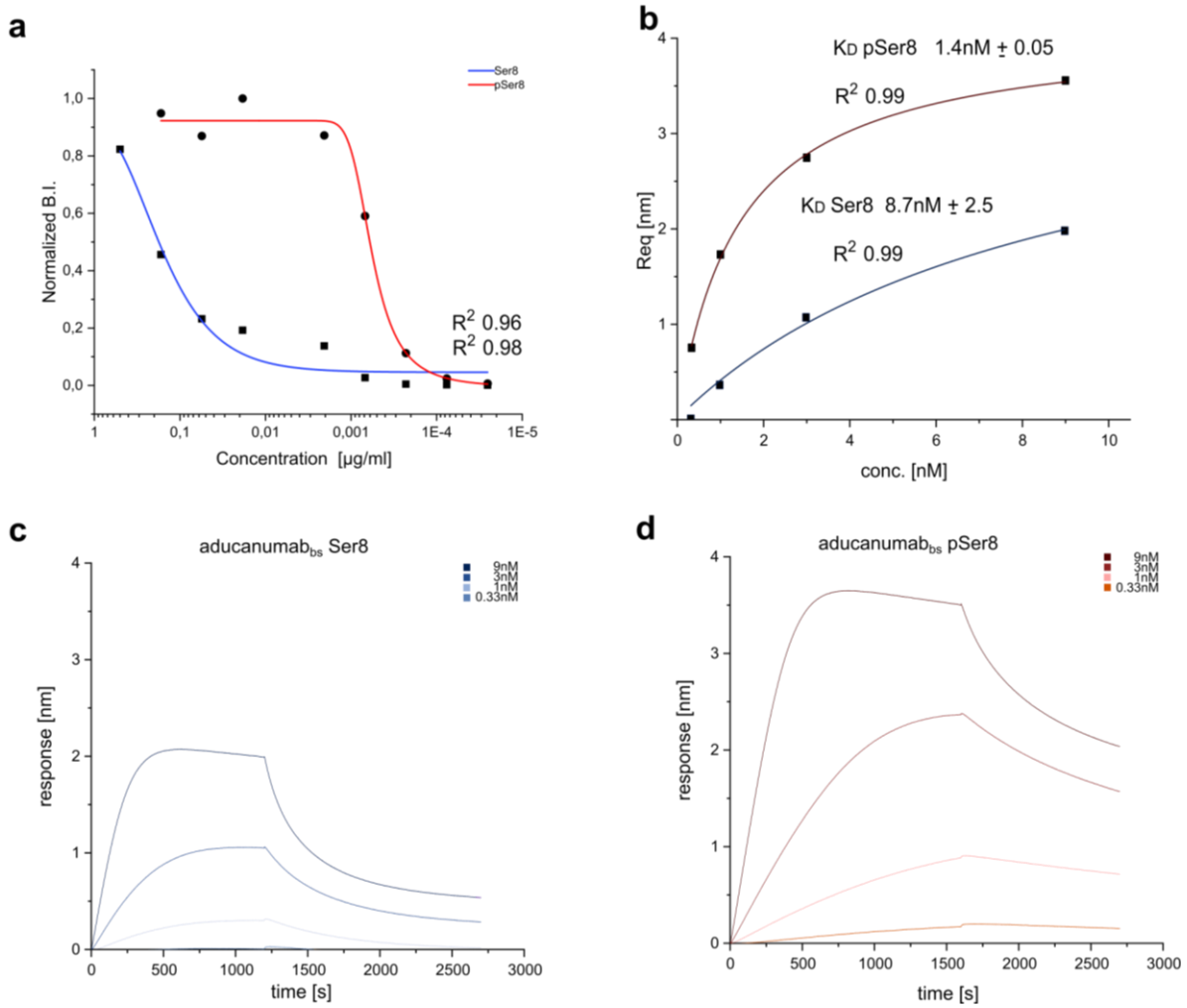

444

445 **Figure 3 – figure supplement 2. Phosphorylation aids Aducanumab$_{bs}$ binding to synthetic**
446 **monomeric Aβ1-15.** (a) Titration of Aducanumab$_{bs}$ at different concentrations to achieve high
447 selectivity for phosphorylated pSer8-Aβ1-15 over unphosphorylated Aβ1-15. The signals were
448 internally normalized and fitted as a sigmoidal curve (Boltzmann). The phospho signal for
449 pSer8-Aβ1-15 is shown in red (r^2 0.98) and the signal for unphosphorylated Aβ1-15 is shown
450 in blue (r^2 0.96). (b) BLI steady-state analysis revealed KDs of 1.4nM and 8.7nM for
451 phosphorylated and unphosphorylated Aβ1-15, respectively (1:1 model). (c) Biolayer
452 interferometry dose-response curve of Aducanumab binding to the NTA-loaded
453 *DAEFRHDSGYEVHHQ-6xHis-amide* peptide. (d) Biolayer interferometry dose-response

curve of Aducanumab binding to the NTA-loaded *DAEFRHDpSGYEVHHQ-6xHis-amide* peptide.

To further explore the relevance of the observed interaction between Aducanumab$_{bs}$ and the N-terminal phosphorylated Aβ fragment, we conducted molecular dynamics (MD) simulations (**Figure 3 – figure supplement 3**) using the published crystal structure of Aβ2-7 and Aducanumab Fab complex (PDB: 6CO3). These simulations were performed using Molecular Operating Environment (MOE) software. Specifically, we investigated two different short Aβ peptide sequences, *AEFRHDS* and *AEFRHDpS*, to examine how phosphorylation at Ser(8) affects the binding stability of the antibody-antigen complex.

By assuming that fewer fluctuations in the system correlate with a higher affinity, these data provide insights into the preferential binding mode of Aducanumab to phosphorylated short N-terminal Aβ fragments. By assuming that fewer fluctuations in the system lead to higher affinity, the root mean square deviation (RMSD) diagrams indicate greater stability (average conformation over 600ns) for the phosphorylated peptide due to its reduced fluctuations (**Figure 3 – figure supplement 3**). Additionally, the phospho group enhances the interaction with extra hydrogen bonds compared to the unmodified peptide (**Figure 3 – figure supplement 3**). Conversely, the non-phosphorylated peptide exhibits more fluctuations (**Figure 3 – figure supplement 3**). Thus, under these conditions, the MD simulation results confirm the findings from the microarray and BLI analyses.

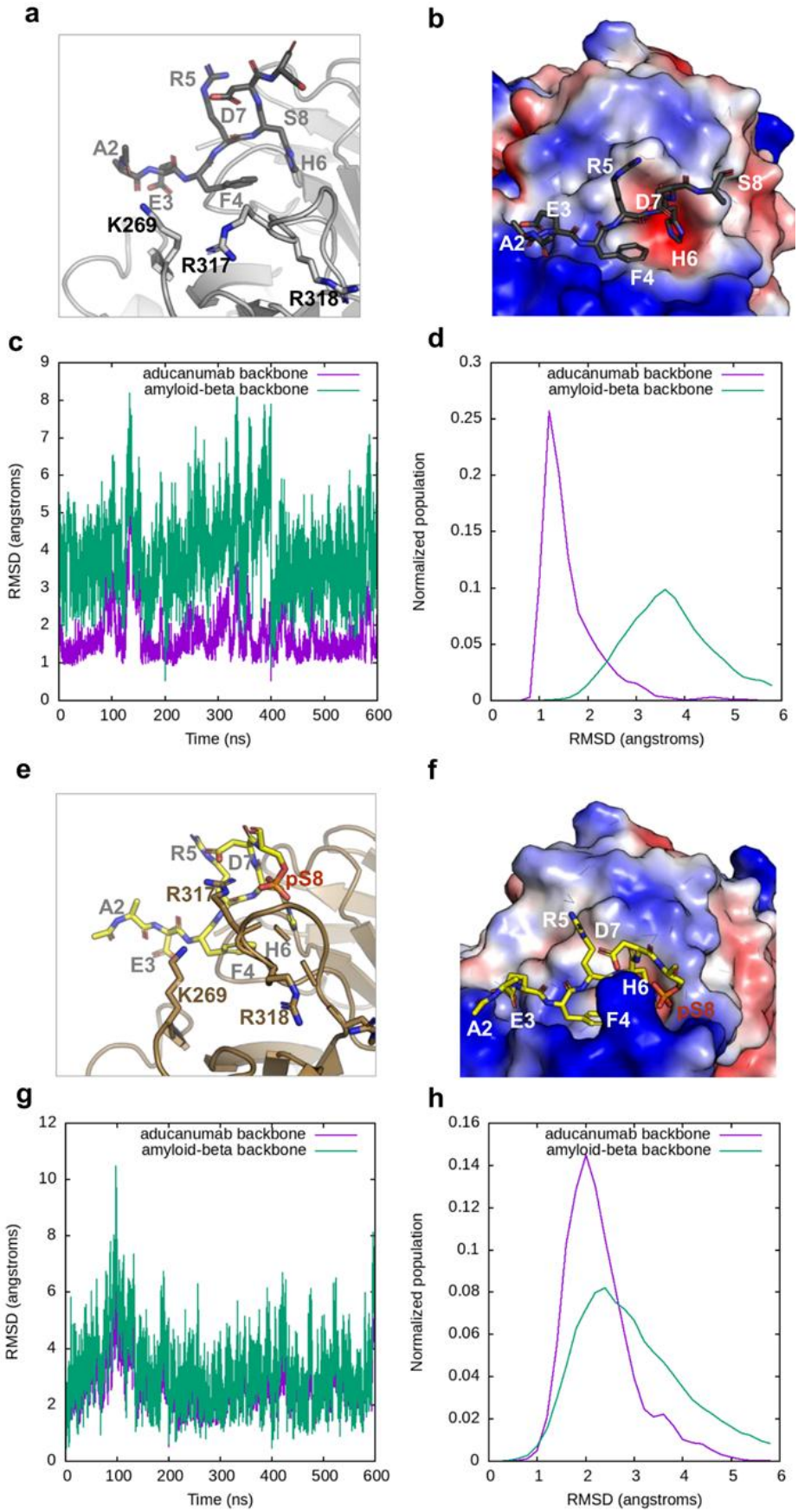

Figure 3 – figure supplement 3. MD simulation of Aducanumab with pSer(8)-Aβ2-8. (a) Sticks and cartoon depiction of the MD simulations between Aducanumab and AEFRHDS. (b)

Electrostatic density for the non-phosphorylated sequence interaction. (c-d) RMSD analysis of the backbone atoms of the unphosphorylated candidate (average conformation over 600ns). (e) Sticks and cartoon depiction of the MD simulations between Aducanumab and AEFRHDpS. (f) Electrostatic density for the pSer8 sequence interaction. (g-h) RMSD analysis of the backbone atoms of the PTM candidate (average conformation over 600ns).

Taken together, the MD simulations rationalize the unexpected preference of Aducanumab$_{bs}$ towards monovalent pSer8Aβ1-15 we observed on microarray. The observation underscores the complexity of Aducanumab$_{bs}$ binding to Aβ. This is further substantiated by comparing the previously resolved structure [41] with the MD simulation for short non-phosphorylated and pSer(8) Aβ-related peptides. Here, pSer8-Aβ2-8, unlike the corresponding non-phosphorylated Aβ, replicates the structurally determined binding mode. In the MD simulation, using the resolved epitope peptide EFRHDpS allows for the binding mode that has R317 and R318 contributing to the paratope. Similarly, the crystal structure (PDB 6CO3) includes a sulfate ion [41] that neutralizes the positive charges of R317 and R318 (**Figure 3 – figure supplement 4**). In summary, the monomeric binding mode benefits from the neutralization of a positive patch on Aducanumab Fab, which likely explains the phospho-preference.

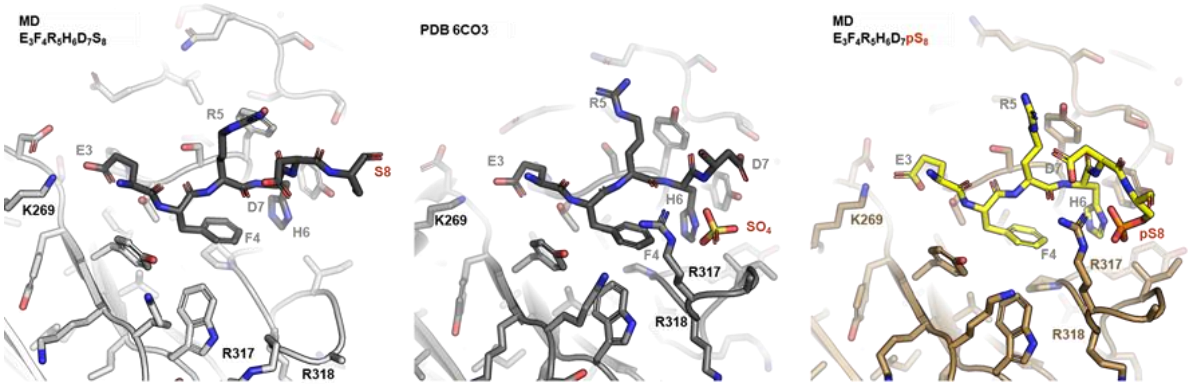

Figure 3 – figure supplement 4. pSer8 but not Ser8-Aβ recapitulate the binding mode resolved by christallography. Comparison of MD simulations with structural data. The MD simulation was conducted with the resolved epitope peptide *EFRHDS,* but in the absence of additional ions, and predicts a largely altered binding mode characterized by over 10 Å movements of R317 and R318. In contrast, the crystal structure (PDB 6CO3) harbors a sulfate ion that neutralizes the positive charge introduced by R317 and R318. Strikingly the MD of the pSer(8) modified peptide recapitulates the resolved X-ray binding mode to monomeric Aβ. Aducanumab targets aggregated Aβ, while still engaging with low micromolar affinity a monomeric Aβ.

Immunoprecipitation with Synthetic and Endogenous Aβ-Peptides Highlights Context-Dependent Aβ-Abs Binding

Thus far, we showed that the initial microarray analysis proved invaluable in defining linear binding motifs, but needs to be complemented in different settings as more complex features of the binding behavior may be missed otherwise. In the following sections, we shift our focus to full-length Aβ peptides, which should reflect the conformations encountered *in vivo* and therefore provide insights into pathophysiologically relevant antibody binding. Thus, the screening results obtained with short Aβ fragments were next extended by analyses with intact Aβx-40 and x-42 variants. Here, the monoclonal Aβ-Abs 4G8, Donanemab$_{bs}$, Lecanemab$_{bs}$, Aducanumab$_{bs}$, and 1E4E11 were tested as representative examples for their capacity in immunoprecipitating specific Aβ variants out of a mixture of ten synthetic Aβ peptides (**Figure 4, Appendix 11-12**). The mixture included Aβ1-40 and 1-42, N-terminal truncated Aβ(2-40, 3-40, pE3-40, 4-40, 5-40, 11-40), N-terminal elongated Aβ(-3-40) and phosphorylated pSer8-Aβ1-40 (amidated C-terminal carboxyl group). The antibodies were covalently coupled to magnetic beads and incubated, separately, with aliquots of the Aβ peptide mixture. After washing the magnetic bead immune complexes, the bound Aβ peptides were eluted, and the immunoprecipitated products were analyzed using MALDI-TOF-MS on TOPAC matrix (**Figure 4A**). As previously established [82], the TOPAC matrix allows for improved detection of phosphorylated Aβ with minimal phosphate loss. Two control antibodies, 4G8 (core epitope 17-21 according to our microarray data) and 1E4E11, were used to set up the system, representing respectively, "pan-Abeta" and pSer8-Aβ1-40 profiles.

The IP-MS signature of 4G8, after incubation with the 10 peptide mix, showed signals from all constituents thus acting as positive control, with major intensities for Aβ5-40, intermediate signals for Aβ4-40, Aβ3-40, Aβ2-40, and Aβ1-40, and only minor signals for Aβ1-42, Aβ(-3-40) and pSer8 Aβ1-40 (**Figure 4A**). Additionally, pyroglutamate AβpE3-40 was clearly recognized by mAb 4G8. As expected from its central epitope 17-21, 4G8 was the only Ab that showed an intense signal for N-terminally truncated Aβ11-40. The monoclonal antibody 1E4E11 preferentially precipitated pSer8-Aβ1-40-amide and, additionally, Aβ2-40, Aβ1-42 and Aβ1-40. The phosphorylated pSer8-Aβ1-40-amide produced the highest signal, suggesting

532 a certain degree of preference (but not specificity) of 1E4E11 for phosphorylated pSer8-Aβ-
533 amide under the tested conditions (**Figure 4A**).

534 In line with the PTM-microarray screening (**Figure 3**), Donanemab$_{bs}$ exhibited highly
535 preferential binding to AβpE3-40, with only minor signals for Aβ3-40 and Aβ2-40 (**Figure**
536 **4A**). The IP-MS spectra obtained with Lecanemab$_{bs}$ showed predominant peaks for Aβ2-40,
537 Aβ1-42, and Aβ1-40 in line with the apparent location of the epitope in the N-terminal region
538 of Aβ (**Figure 4A**). However, synthetic Aβ peptides may display different properties than
539 authentic Aβ peptides in biological samples, such as human cerebrospinal fluid (CSF).
540 Importantly, Lecanemab was previously shown to have a strong preference for Aβ protofibrils
541 and to bind Aβ monomers only weakly [83]. To test whether Lecanemab$_{bs}$ was able to
542 immunoprecipitate endogenous soluble Aβ from a relevant biological sample, we repeated the
543 Lecanemab$_{bs}$ IP-MS experiment with 250 µL of pooled CSF. In the resulting IP-MS spectrum,
544 Aβ1-40, Aβ1-38, Aβ42, Aβ1-37 and Aβ1-39 were detected, albeit with relatively low signal
545 intensities (**Figure 4B**). IP-MS from pooled CSF with Aducanumab$_{bs}$ did not produce any Aβ
546 signals (**Figure 4B**). In contrast, using the mix of ten synthetic Aβ peptides for Aducanumab$_{bs}$
547 magnetic bead IP, we observed clear signals for Aβ2-40, Aβ1-42, Aβ1-40, but not for
548 phosphorylated pSer8-Aβ1-40-amide (**Figure 4A).** This was in contrast to the binding data
549 from array and BLI towards the minimal monovalent epitopes (**Figure 3 – figure supplement**
550 **2 and 3).**

551 For Aducanumab$_{bs}$, microarray, BLI and IP-MS data suggest three binding modes. One
552 presumably aggregation specific site (*EFRHDS*) as predicted by previous molecular dynamics
553 studies [84], primarily via neutral V_L, where the Ser(8) would only contact the Tyr-92 [84], in
554 line with previous data [41]. A second binding site (EFRHDpS) relevant for the binding of
555 short synthetic N-terminal Aβ fragments as resolved by our pSer(8) MD primarily contacting
556 the positively charged V_H chain paratope via Arg-317-318 and in agreement with the sulfate
557 ion-containing structure (**Figure 3 – figure supplement 4)**. Lastly, in a similar way the binding
558 of Aducanumab to monomeric A*EFRHDS* (Aβ2-8) can benefit from the presence of negatively
559 charged sulfate ions [41] (pdb: 6CO3). Of note, a recent molecular dynamics study suggested
560 the presence of an N-terminal neutral domain in Aβ protofibrils (Aβ:Fab contact Ser8:Tyr92)
561 [34], which may contribute for the preferential binding of Aducanumab to aggregated forms of
562 Aβ.

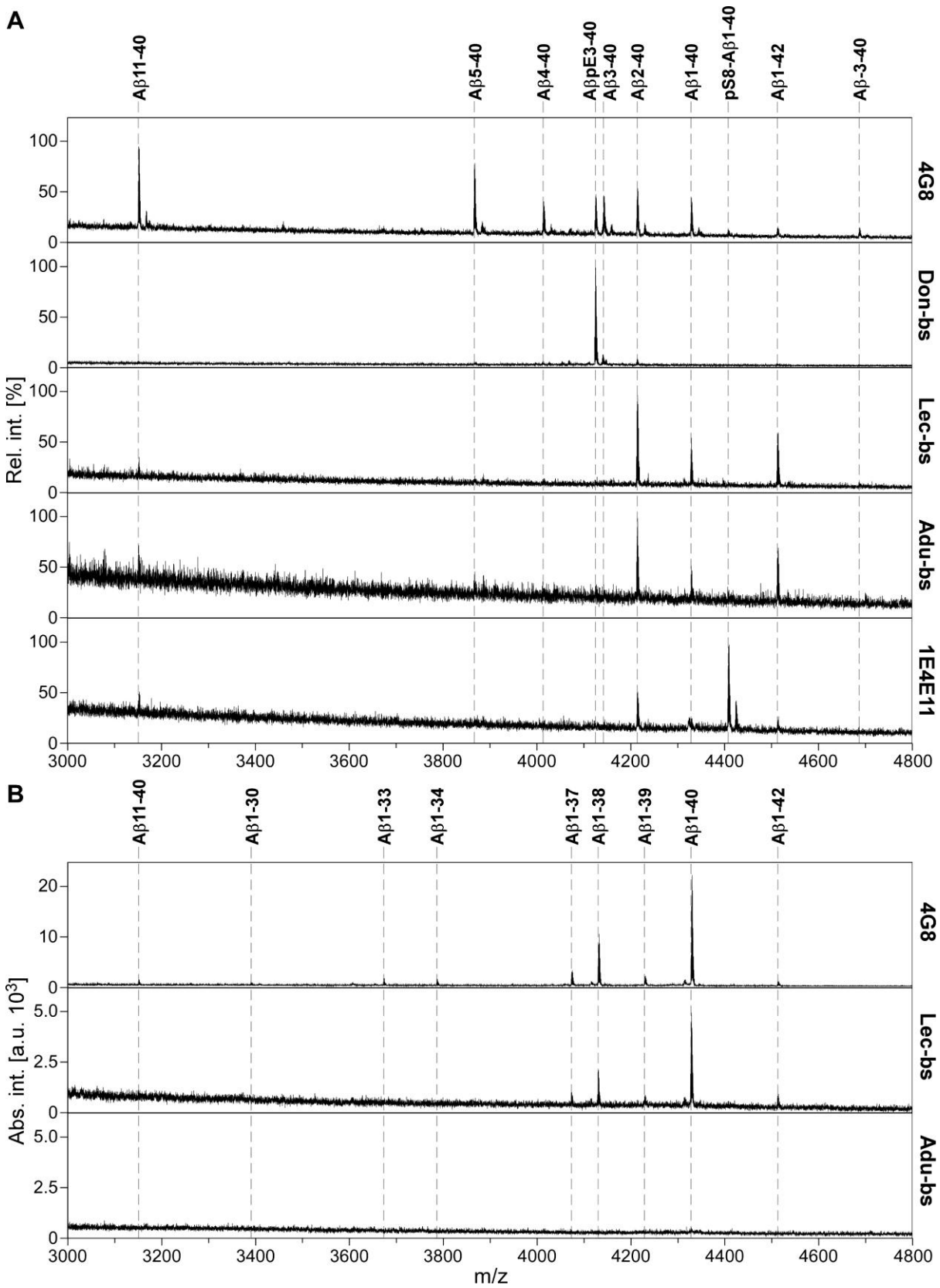

Figure 4: IP-MS signature of different biosimilar Aβ-Abs. (A) A mixture of synthetic Aβ peptides was immunoprecipitated with the following Aβ-Abs (from top to bottom): 4G8 (pan-antibody), Donanemab$_{bs}$ (Don-bs), Lecanemab$_{bs}$ (Lec-bs), Aducanumab$_{bs}$ (Adu-bs), and

567 1E4E11 (phospho-selective control). Mass spectra were generated by MALDI-TOF-MS in
568 reflector mode from TOPAC matrix and are representative for two independent experiments.
569 We noted that the signal pattern slightly varied between experiments, which we mainly
570 attributed to some immunoprecipitation of co-aggregated Aβ species, an effect that has to be
571 considered under the experimental conditions applied. (B) IP-MS from pooled human CSF
572 using MALDI-TOF-MS from conventional CHCA matrix. Mab 4G8 (positive control) and
573 Lecanemab$_{bs}$, but not Aducanumab$_{bs}$ immunoprecipitated authentic biological Aβ peptides
574 from pooled human CSF under the tested conditions. Major peaks were observed for Aβ1-40
575 and Aβ1-38. The spectra shown are representative for two replicate measurements each from
576 two independent immunoprecipitations.

577 Aggregation-Dependent Binding of Biosimilar Aβ-Abs in vitro and 578 in AD brain tissue

579 To further complement the characterization of the biosimilar Aβ-Abs, we applied gel
580 electrophoretic separations of Aβ peptides followed by Western blotting, automated Capillary
581 Isoelectric Focusing immunoassays (CIEF-immunoassay) with charge-based separation of Aβ
582 peptides, and immunohistochemistry (IHC) experiments on brain tissue with pre-adsorption of
583 Aβ-Abs.

584 Aducanumab and Lecanemab preferably bind specific aggregated forms of Aβ over monomeric
585 forms [38,40,41][38,83]. In agreement with these reports, our analysis showed that
586 Aducanumab$_{bs}$ clearly detected highly aggregated fibrillar Aβ1-42 on Bistris-SDS gradient
587 PAGE/Western blot. In contrast, it generated essentially no appreciable signals with
588 monomerized hexafluoroisopropanol (HFIP)-treated or oligomeric Aβ1-42 preparations under
589 the tested conditions (**Figure 5A**). On peptide Bicine-Tris SDS-PAGE/Western blot and on
590 CIEF-immunoassays we observed substantial variances with Aducanumab$_{bs}$ between different
591 experiments (data not shown), making reliable interpretations difficult [85]. The observed high
592 variance of the Aducanumab$_{bs}$ results on CIEF-immunoassay and peptide SDS-PAGE/Western
593 blot might be related to the low affinity of Aducanumab for monomeric Aβ [41] and the
594 possibility that Aβ dimers or low order oligomers might form during the experiment [85]. In
595 good agreement with the strong preference of Aducanumab$_{bs}$ for highly aggregated fibrillar Aβ
596 (see above), pre-adsorption with fibrillar Aβ1-42 largely blocked Aducanumab$_{bs}$
597 immunoreactivity of vascular and parenchymal Aβ deposits in AD brain tissue, in contrast to
598 pre-adsorption with an excess of Aβ1-42 monomers (**Figure 5B**).

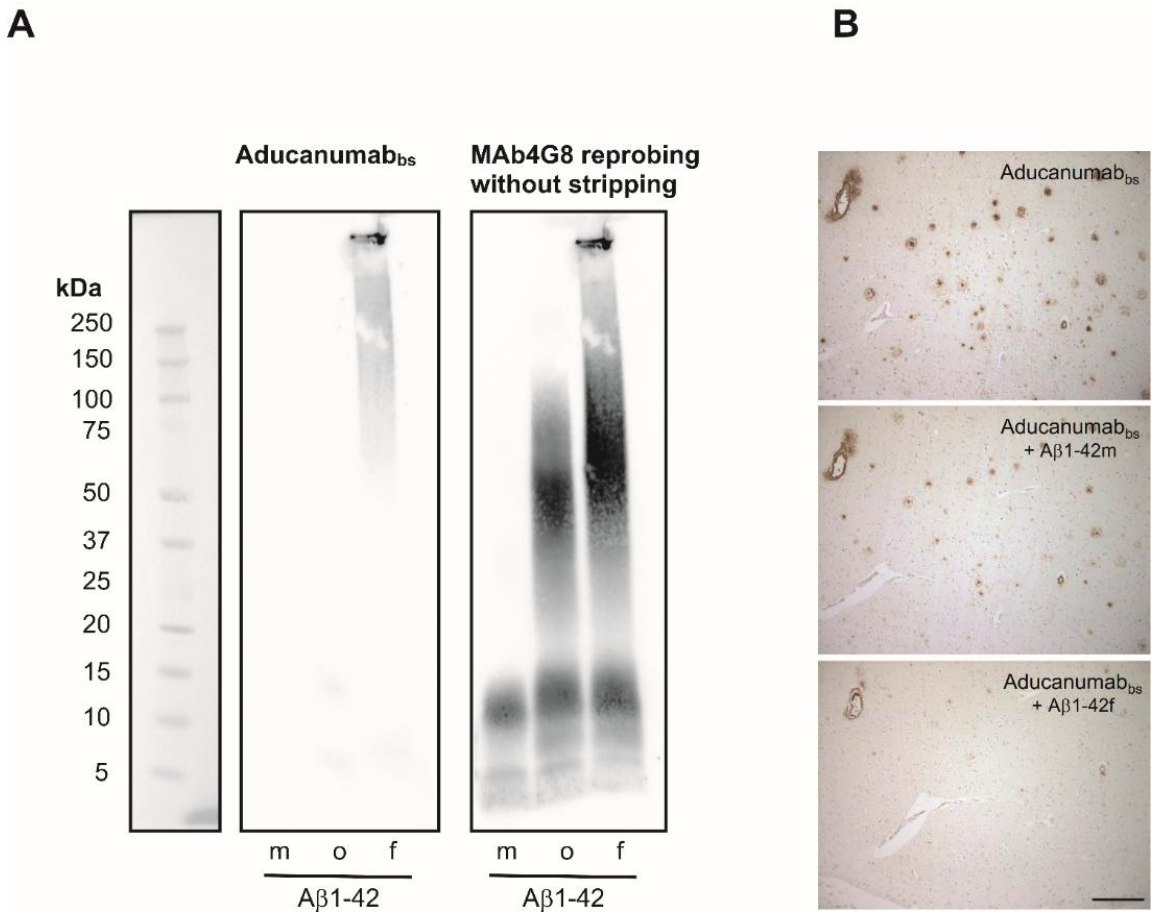

Figure 5: **Aducanumab$_{bs}$ shows strong preference for highly aggregated fibrillar Aβ1-42**. (A) HFIP-treated Aβ1-42 monomer (m), oligomer (o) and fibril preparations (f) (1.44 µg each) were separated by 4-12% Bistris SDS-PAGE, blotted onto nitrocellulose and probed with Aducanumab$_{bs}$ (5 min exposure, F 0.84, image display: High: 65535; Low: 0; Gamma: 0.85). Following image recording the blot membrane was reprobed without prior stripping (no removal of primary and secondary antibodies) with mAb4G8 (1 min exposure, image display: High: 54971; Low: 0; Gamma: 0.99). That way the 4G8 signals were essentially added on top of the initial Aducanumab$_{bs}$ signals and background artifacts. The positions of pre-stained protein marker bands on the blot membrane are shown on the left-hand side. (B) Parallel sections from an AD patient were stained with Aducanumab$_{bs}$ and Aducanumab$_{bs}$ that had been pre-adsorbed with either Aβ1-42 monomers (Aβ1-42m) or Aβ1-42 fibrils (Aβ1-42f). Scale bar: 200 µm.

Lecanemab$_{bs}$ recognized Aβ1-40, Aβ1-42, Aβ3-40 (pI approximately 5.97) Aβ-3-40 (aka. APP669-711),phosphorylated pSer8-Aβ1-40on CIEF-immunoassay and Bicine-Tris SDS-PAGE/ Western blot, thus recapitulating the initial microarray mapping for Lecanemab$_{bs}$ shown in **Figure 1**. It appears, that under these experimental conditions Lecanemab$_{bs}$ can bind to an epitope located in the N-terminal region of the Aβ sequence. On gradient Bistris SDS-PAGE/Western blot and under the tested conditions, Lecanemab$_{bs}$ showed a certain, but not absolute preference for aggregated forms of Aβ1-42 over monomeric and low-n oligomeric forms in the HFIP-treated Aβ1-42 preparation (**Figure 6**). The immunohistochemical detection

620 of Aβ in vascular and parenchymal deposits by Lecanemab$_{bs}$ in brain sections from an AD-
621 patient was efficiently blocked by antibody pre-adsorption with monomerized, oligomeric and
622 fibrillar preparations of Aβ1-42 (**Figure 6E**). However, it cannot be excluded, that the HFIP
623 treated Aβ1-42 monomers aggregated during the experiment.

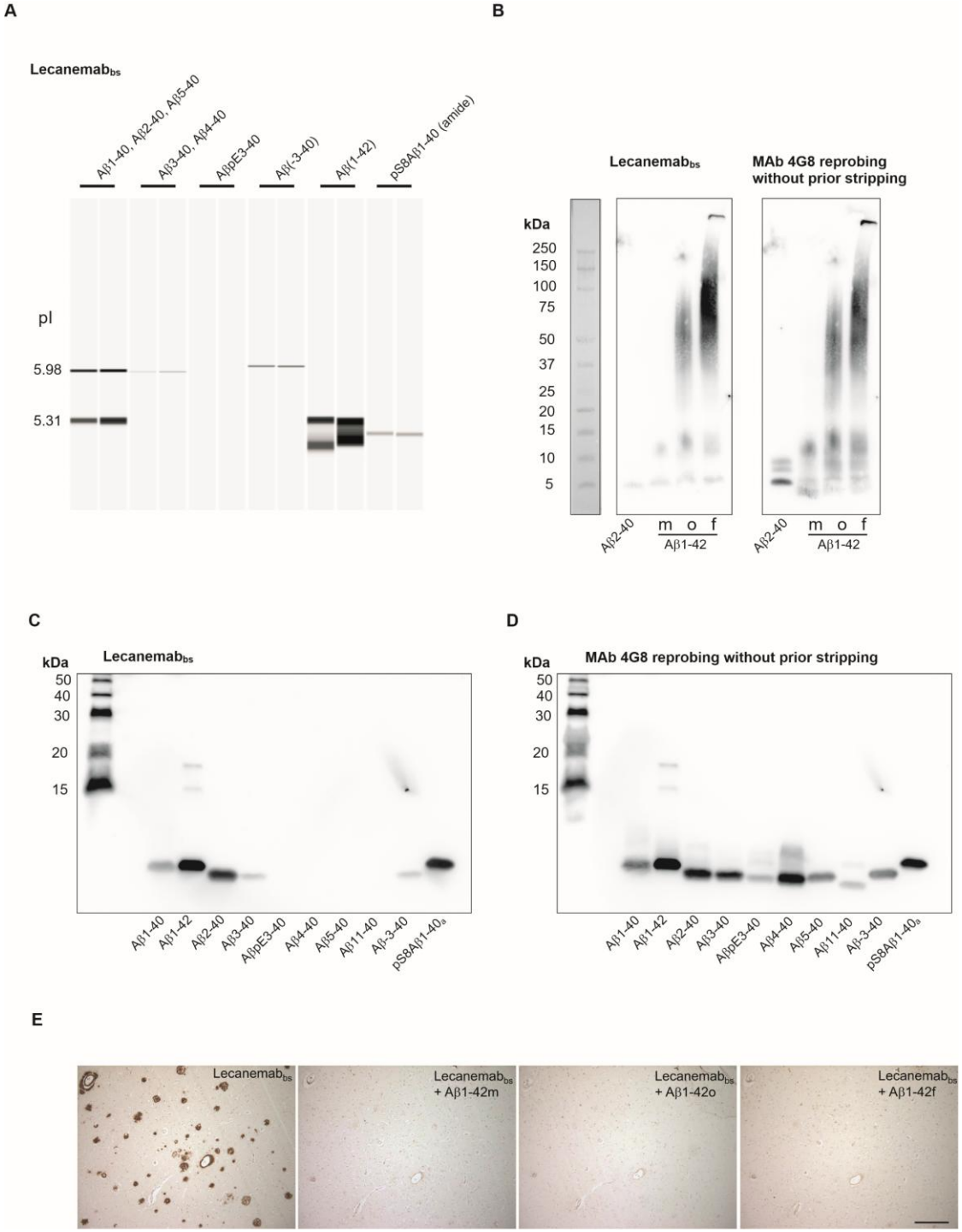

624

625 **Figure 6**: **Lecanemab$_{bs}$ recognizes an epitope located in the N-terminal region.** (A) shows
626 an example of CIEF-immunoassay results for Lecanemab$_{bs}$ displayed as lane view (Western
627 blot simulation). The indicated Aβ peptides were separated by isoelectric focusing in
628 microcapillaries on a Peggy Sue device, immobilized photochemically to the inner capillary
629 wall and subjected to immunological detection. Under the tested conditions, Lecanemab$_{bs}$

630 detected Aβ1-40 (pI 5.31), Aβ2-40 (pI 5.98), Aβ3-40 (pI 5.97), Aβ-3-40 (pI 6.04), Aβ1-42 (pI
631 approx. 5.3) and pSer8Aβ1-40 (amide) (pI 5.13-5.14). (B) Synthetic Aβ2-40 (361 ng), and
632 monomerized (m), oligomeric (o) and fibrillar (f) preparations of Aβ1-42 (361 ng of each) were
633 separated by 4-12% Bistris SDS-PAGE, blotted onto nitrocellulose and probed with
634 Lecanemab$_{bs}$ (0.5 µg/mL). Exposure: 2 min 7.5 sec; F 0.84; image display: high: 47545; low:
635 0; gamma: 1.0. After blot development, the blot membrane was reprobed with mAb 4G8
636 without prior stripping. That way the 4G8 signals were essentially added on top of the initial
637 Lecanemab$_{bs}$ signals and background artifacts. Exposure: 1 min F 0.84; image display: high:
638 46277; low: 0; gamma: 1.0. (C) The indicated Aβ peptides (50 ng of each) were separated by
639 Bicine Tris (peptide) SDS-PAGE, blotted on PVDF, and probed with Lecanemab$_{bs}$. Exposure:
640 5 min F 0.84, image display: high: 65535; low: 0; gamma: 0.85. (D) To confirm loading and
641 successful blotting of all Aβ peptides, the blot membrane was re-probed with mAb 4G8 without
642 prior stripping (see above). Exposure: 5 min F 0.84; image display: high: 65535; low: 0;
643 gamma: 1.0. (E) Parallel sections from an AD patient were stained with Lecanemab$_{bs}$ and
644 Lecanemab$_{bs}$ that had been pre-adsorbed with either Aβ1-42 monomers (Aβ1-42m), Aβ1-42
645 oligomers (Aβ1-42o) or Aβ1-42 fibrils (Aβ1-42f). Scale bar: 200 µm.

646 C-Terminal Aβ Elements Contribute to Lecanemab-Binding in 647 Tissue

648 To investigate in more detail the dependence of Lecanemab$_{bs}$ binding on the Aβ peptide length
649 and presumed resulting conformational differences, we performed additional pre-adsorption
650 assays using a series of C-terminal truncated Aβ peptides with an intact N-terminal epitope.
651 Since the original Lecanemab biosimilar antibody (Proteogenix Cat. No PX-TA1746) was not
652 available anymore, Lecanemab$_{bs}$ obtained from a different source (BioXCell (#BXC-SIM0032
653 / InVivoSIM) was used. Again, preincubation with Aβ1-42 monomers (Stressmarq) completely
654 blocked Lecanemab$_{bs}$ binding, whereas shorter peptides such as Aβ1-16, Aβ1-34 and Aβ1-38
655 did not. Thus, it appears that an intact N-terminus alone is not sufficient for Lecanemab$_{bs}$
656 recognition, suggesting that additional elements contribute to Lecanemab binding of oligomers
657 and aggregates.

658 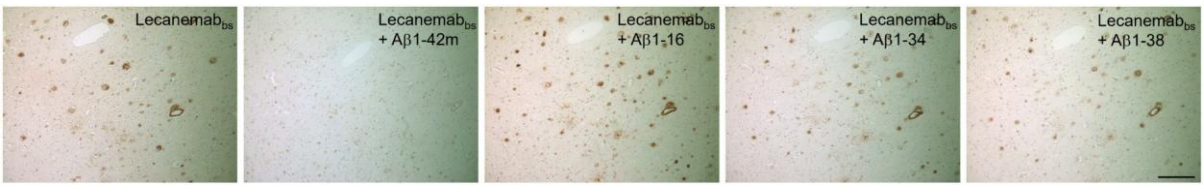

659 **Figure 6 – figure supplement 1. HFIP treated Aβ1-42, but not shorter synthetic Aβ-**
660 **peptides block Lecanemab$_{bs}$ binding to amyloid plaques.** Parallel sections from an AD
661 patient were stained, from left to write, with Lecanemab$_{bs}$ only (BioXCell #BXC-SIM0032) or
662 pre-adsorbed with either Aβ1-42 monomers (Aβ1-42m), Aβ1-16 (Aβ1-16), Aβ1-34 (Aβ1-34)
663 and Aβ1-38 (Aβ1-38). Scale bar: 200 µm.

664

665 On CIEF-immunoassay and Bicine-Tris SDS-PAGE/Western blot, Donanemab$_{bs}$ detected
666 AβpE3-40 and Aβ3-40 (both at a pI of approximately 5.95 on CIEF immunoassay) with a clear
667 preference for the Aβ variant starting with the cyclized N-terminal pE. Other N-terminal Aβ
668 variants that were tested produced no or very small signals (**Figure 7 B, C**). On gradient Bistris
669 SDS-PAGE/Western Blot, Donanemab$_{bs}$ detected multiple AβpE3-40 bands in the low
670 Mwrange, presumably representing monomers and low order oligomers which were formed
671 during sample preparation or SDS electrophoresis [85]. The HFIP-treated monomeric,
672 oligomeric and fibrillar Aβ1-42 preparations produced very faint signals with Donanemab$_{bs}$
673 (**Figure 7D**). Re-probing of the blot (without stripping) with mAb4G8 showed multiple Aβ1-
674 42 bands in the low molecular weight range (<15 kDa) in the HFIP-treated preparation
675 (presumably monomers and low order oligomers). The Aβ1-42 oligomer preparation showed
676 a similar pattern of bands smaller than 15 kDa and between 25 and 100 kDa. The Aβ1-42 fibril
677 preparation showed low order oligomeric Aβ1-42 bands, in the molecular weight range of 37.5
678 to 150 kDa as well as highly aggregated Aβ1-42 which, unable to enter the stacking gel. On
679 immunohistochemistry, the detection of Aβ vascular and parenchymal deposits by
680 Donanemab$_{bs}$ in AD brain sections was efficiently suppressed by pre-adsorption of the
681 antibody with synthetic AβpE3-40, but not with Aβ1-40 or Aβ3-40 peptides (**Figure 7E**).

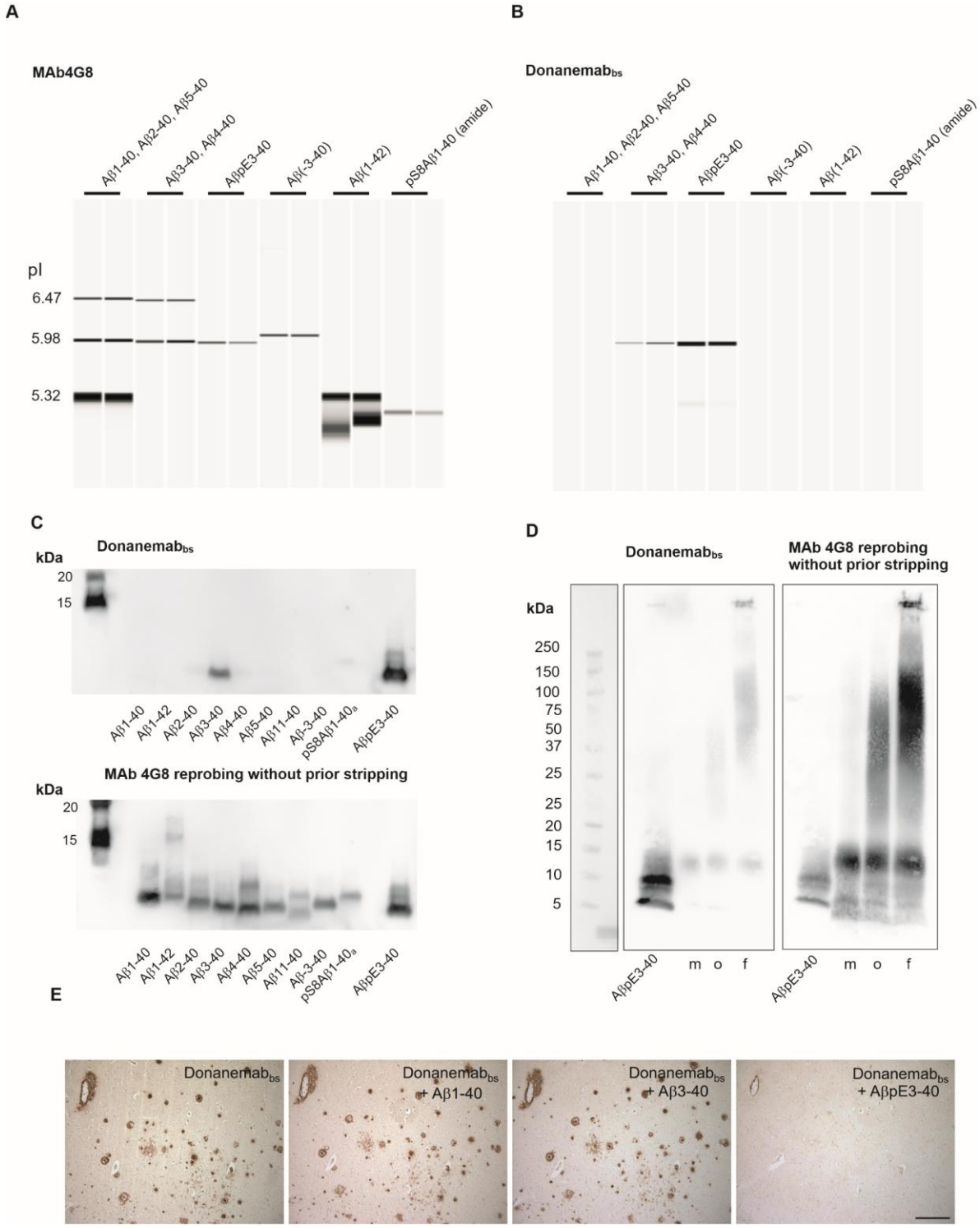

Figure 7: Donanemab$_{bs}$ shows high preference for pyroglutamate bearing pEAβ3-40. The upper panel shows lane views (Western blots simulation) of a CIEF-immunoassay for assessing the detection of different Aβ variants by (A) mAb 4G8 (positive control antibody) and (B) Donanemab$_{bs}$. The indicated Aβ variants were separated by isoelectric focusing in microcapillaries on a Peggy-Sue device, immobilized photochemically to the inner capillary wall and subjected to immunological detection by (A) mAb 4G8 and (B) Donanemab$_{bs}$. (C) Synthetic Aβ peptides (50 ng per lane) were separated by Bicine Tris (peptide) SDS-PAGE, blotted on PVDF and probed with Donanemab$_{bs}$ (0.5 µg/mL) (upper image). Exposure: 5 min F 0.84; image display: high: 59406; low: 0; Gamma: 0.65. To confirm that all Aβ variants were

692 loaded and blotted, the blot membrane was reprobed with mAb 4G8 without prior stripping.
693 That way, the 4G8 signals were essentially added on top of the initial Donanemab$_{bs}$ signals and
694 background artifacts (lower image). Exposure: 5 min F 0.84; image display: high: 65535; low:
695 0; gamma: 0.77. (D) AβpE3-40 and Aβ1-42 monomer (m), oligomer (o) and fibril preparations
696 (f) were separated by 4-12% Bistris SDS-PAGE, blotted onto nitrocellulose and probed with
697 Donanemab$_{bs}$ (image display: High: 64091; Low: 0; Gamma: 0.75), followed by reprobing
698 without prior stripping with mAb4G8 (image display: High: 46984; Low: 0; Gamma: 1.0). The
699 positions of prestained protein marker bands on the blot membrane are shown on the left-hand
700 side. (E) A pre-adsorption experiment employing synthetic Aβ peptides in human AD brain
701 tissue showed that the immunoreactivity of Donanemab$_{bs}$ was not suppressed by pre-adsorption
702 of the antibody with excess amounts of synthetic Aβ1-40 and Aβ3-40 peptides. In contrast, a
703 pre-incubation with AβpE3-40 effectively attenuated the antibody signal in extracellular Aβ
704 deposits as well as in the vasculature.

705 Conclusion

706 The exact binding specificity of Aβ-Abs, and its dependence on sequence context and
707 aggregation state, is central both for their use as research tools and for their evaluation and
708 development as therapeutic and diagnostic agents. Here we combined high-density peptide
709 microarray analysis with complementary methodologies to generate a comprehensive dataset
710 for 20 research and biosimilar Aβ-Abs. In total, 20,000 peptide–antibody interactions resolved
711 individual epitopes at single–amino-acid resolution and clarifying the influence of PTMs and
712 amino-acid exchanges for all epitopes within a unified experimental setup. The array analyses
713 were complemented by IP-MS, CIEF immunoassay, SDS-PAGE/Western blot, and
714 immunohistochemistry studies, thereby linking fine epitope definition and profiling with
715 binding of full-length Aβ under native and aggregated conditions.

716 Comparative analyses highlighted clear mechanistic differences between the three therapeutic
717 antibodies. For Donanemab, screening of monovalent peptides consistently recapitulated a core
718 epitope at residues 3–10, with cyclized AβpE3-x as the dominant binding determinant. In
719 contrast, Lecanemab and Aducanumab both required aggregated Aβ for full binding activity
720 but mapped to overlapping N-terminal sequences (residues 3–7 for Lecanemab; 2–7 for
721 Aducanumab). Binding quantification further substantiated a preference of Aducanumab for
722 Ser8-phosphorylated Aβ for non-aggregated forms, and a marked sensitivity to the familial
723 H6R mutation, consistent with recent reports linking antibody efficacy to differences between
724 soluble and aggregated Aβ pools [86]

725 The qualitative and quantitative binding data, together with our molecular dynamics
726 simulations and the previous structural reports, provide a mechanistic explanation for the

observed binding requirements. For Aducanumab, X-ray crystallography revealed a Fc-mediated dimer interface that stabilises binding to aggregated Aβ [41]. This dimerisation also explains our observed preference for pSer8-modified Aβ monomers: phosphorylation neutralises the Arg-Ala-Arg motif at the Fc-dimer interface, thereby promoting dimerisation and avidity-enhanced binding. In aggregated Aβ forms, such phosphorylation is dispensable because avidity is already provided by multimerisation, reconciling our peptide library, BLI, and tissue binding results with structural models and simulations of Aducanumab [41, [84],93]. For Lecanemab, our binding profiles align closely with the model proposed on the basis of D3 antibody similarity (PDB 5MY4) [93], correctly accounting for sequence tolerances at positions 3–7. However, in contrast to published claims [93], we find no evidence that N-terminal extensions beyond Glu3 reduce affinity. Binding is preserved both in vitro and in AD tissue, supporting a minimal epitope definition that includes residues 3–7, consistent with our peptide, MS, and immunohistochemistry data [38,93], and with recent demonstrations of Lecanemab's preferential binding to fibrillar Aβ aggregates [46].

In summary, we systematically compared the binding requirements of 20 Aβ-Abs, addressing sequence (including genetic and species variants), PTM, and structural aspects. By resolving discrepancies between structural models and biochemical data, we provide mechanistic insight into the distinct binding modes of Aducanumab and Lecanemab, and into the strict selectivity of Donanemab. This work provides a resource for the rational selection of Aβ-Abs in research and diagnostics and may help inform the evaluation and design of future therapeutic and diagnostic Aβ-Abs.

Methods

Ethics approval and patients consent

In this study, a pooled CSF sample prepared from several individual CSF samples from the local biobank at the Department of Psychiatry and Psychotherapy at the University Medical Center Göttingen was used in some IP-MS experiments. The collection and archiving of biological samples and clinical data in strictly pseudonymous form in a local biobank and their use in biomarker research were approved by the ethics committee of the University Goettingen (Protocol number 9/2/16). From all participants or their legal representatives written informed consent was obtained prior to the inclusion in the biobank. All study participants received detailed information prior to enrolment in the study and collection of the biomaterial. In addition, an information sheet was handed out by the study physicians at the Department of Psychiatry and Psychotherapy at the University Medical Center Göttingen. After a possible reflection period, written informed consent was obtained from the study participants. If the ability to consent was not given, a separate informed consent form was also provided for the study participant's legal representative, and the legal representative signed the informed consent form for the study. All procedures involving human participants were in accordance with the ethical standards of the institutional and/or national research committee and with the 1964 Helsinki declaration and its later amendments or comparable ethical standards.

Paraffin-embedded human brain samples from individuals with sporadic Alzheimer's disease (AD) were obtained from the Netherlands Brain Bank (NBB,Netherlands Institute for Neuroscience, Amsterdam (open access: www.brainbank.nl)). All material has been collected from donors for or from whom a written informed consent for a brain autopsy and the use of material and clinical information for research purposes had been obtained by the NBB. For the -analyses in the present study, sections from the medial frontal gyrus region of the brain were utilized. All procedures involving human tissue were approved by the ethical committee at the University Medical Center Göttingen (Protocol number 12/1/15).

Preparation of Functionalized Cellulose Discs

Paper functionalization was performed by introducing some variations to the previous protocol [87] aimed at increasing the output of discs per session. In brief, Whatman paper grade 50 (45 × 25 cm) was cut into 4mm diameter discs using an OMTech 50-watt CO2 laser at 7.8% power

779 and 150 mm/s speed. To reduce mechanical stress and facilitate transfer into a 384-plate, each
780 disc was cut with a semi-circular pattern. The pre-cut layout (15 x 10 cm) was then treated for
781 3 hours with a solution of 9-fluorenylmethyloxycarbonyl-β-alanine (Fmoc-β-Ala-OH),
782 diisopropylmethanediimine (DIC) and 1-Methylimidazole (NMI). The Fmoc absorption of
783 each batch of functionalized cellulose membrane was determined at 290nm after 20 minutes of
784 deprotection with 20% (v/v) piperidine (pip) in DMF. The average loading was 130nmol/disc.

785 Microarray Synthesis

786 The µSPOT assay was performed as previously described [88]. First, the APP sequence
787 (UniProtKB: P05067) was displayed in microarray format as 15mer overlapping peptide
788 library. Peptide arrays were synthesized [89-91] using MultiPep RSi robot (CEM GmbH,
789 Kamp-Lintford, Germany) on cellulose discs containing Fmoc-β-Ala linkers. Natural amino
790 acid building blocks were purchased from IRIS (IRIS Biotech GmbH, Marktredwitz,
791 Germany). Special building blocks employed in this study such as isomers, stereoisomers,
792 phosphorylation and pyroglutamination post-transcriptional modifications are listed here:
793 Fmoc-L-Ser(PO(OBzl)OH)-OH (Iris – FAA1423), L-Pyroglutamic acid pentachlorophenyl
794 ester (Novabiochem - 8.54203), Fmoc-L-Asp-OtBu (Iris – FAA1356), Fmoc-D-Asp-OtBu
795 (Carbosolutions – CC05095) and Fmoc-D-Asp(tBu)-OH (Iris – FAA1309). Synthesis was
796 carried out by deprotecting the Fmoc-group using 20% piperidine in dimethylformamide
797 (DMF). Peptide chains were elongated using a coupling solution consisting of amino acids
798 (0.5M) with oxyma (1M) and DIC (1M) in DMF (1:1:1). Coupling steps were carried out 3
799 times (30min), followed by capping (4% acetic anhydride in DMF). Discs were transferred into
800 96 deep-well plates for the work-up. Side chains were deprotected using 90% trifluoracetic
801 acid (TFA), 2% dichloromethane (DCM), 5% H_2O and 3% triisopropylsilane (150µL/well) for
802 1h at room temperature (RT). Afterward, the deprotection solution was removed, and the discs
803 were solubilized ON at RT, while shaking, using a solvation mixture containing 88.5% TFA,
804 4% trifluoromethanesulfonic acid (TFMSA), 5% H2O and 2.5% TIPS (250µL/well). The
805 resulting peptide-cellulose conjugates (PCCs) were precipitated with ice-cold ether
806 (700µL/well) and spun down at 2000×g for 10min at 4°C, followed by two additional washes
807 of the formed pellet with ice-cold ether. The resulting pellets were dissolved in DMSO
808 (250µL/well).

809 # Microarray Quality Control

810 LC-MS was carried out using peptide quality controls that were cleaved from solid support. To
811 ensure cleavage, a Rink amide linker (Iris) suitable for SPPS on cellulose support was
812 introduced during the first coupling cycle. In an acidic environment, the quality controls were
813 cleaved off from the solid support. To isolate the quality controls, 150 µL of the supernatant
814 (SN) was transferred to 1.5 mL reaction tubes, followed by the addition of 700 µL of diethyl
815 ether. The samples were then vortexed, and the peptides were allowed to precipitate by
816 incubation at -20°C overnight. After centrifugation at 13,300 × g and 4°C for 10 min, the SN
817 was discarded, and 500 µL of diethyl ether was added. The mixture was vortexed, centrifuged
818 for 10 min, and the supernatant was decanted. This process was repeated twice, and the peptides
819 were left to dry for 60 min. Finally, the Rink amides were dissolved in 50 µL of 50%
820 acetonitrile: 0.1% formic acid (v/v) and vortexed briefly before centrifugation at 13,300 × g
821 and room temperature. For analysis, the quality controls were diluted 1:3 and sent to LC-MS
822 (Agilent technologies).

823 # Microarray Printing

824 PCCs solutions were mixed 2:1 with saline–sodium citrate buffer (150mM NaCl, 15mM
825 trisodium citrate, pH7.0) and transferred to a 384-well plate. For transfer of the PCC solutions
826 to white-coated CelluSpot blank slides (76×26mm, Intavis AG Peptide Services GmbH and
827 CO. KG), a SlideSpotter (CEM GmbH) was used. After completion of the printing procedure,
828 slides were left to dry ON.

829 # Microarray Binding Assay

830 The microarray slides were blocked for 60min in 5% (w/v) skimmed milk powder (Carl Roth)
831 0.05% Tween20 phosphate-buffered saline (PBS; 137mM NaCl, 2.7mM KCl, 10mM
832 Na_2HPO_4, 1.8mM KH_2PO_4, pH7.4). After blocking, the slides were incubated for 30 min with
833 a solution of blocking buffer and monoclonal and polyclonal Aβ-Ab (**Table 1**). They were then
834 washed 3× with PBS 0.05% Tween20 for 1min. IgG antibodies were detected using goat anti
835 mouse IgG-HRP (Thermo Fisher Cat. No31430), Goat anti-Rabbit IgG, Antibody, HRP (Cell
836 Signaling: 7074), Goat anti-Rat IgG (H+L) Secondary Antibody, HRP (TF: 31470) and Goat
837 anti-Human IgG (H+L) Secondary Antibody, HRP (TF: 31410). The chemiluminescence
838 readout was detected with an Azure imaging system c400 (lowest sensitivity, 1s, 5s, 10s, 30s,

1m, 2m) using SuperSignal West Femto maximum sensitive substrate (Thermo Scientific GmbH, Schwerte, Germany). The raw grayscale intensities were measured using open-source MARTin software [92].

Dot Blot

The purified peptides were printed onto white-coated CelluSpot blank slides using the Slide Spotter at a starting amount of 0.05 µg. The slides were allowed to dry for 3 hours and rinsed once with 1X PBS to remove the unbound peptides. After blocking in 5% (w/v) skimmed milk powder for 1 hour, the slides were incubated with 1nM Aducanumab$_{bs}$ and IgG signals were detected using goat anti-human IgG DL650 (1:1000 - Invitrogen 84545). The fluorescence signal readouts were acquired using Amersham Image Quant 800 (GE Healthcare) with an exposure time of 30 seconds and 4x4 binning.

Molecular Dynamics Simulations

For molecular dynamic (MD) simulations the crystal structure of the aducanumab Aβ complex structure (PDB: 6CO3) was used. The complex structure was prepared using MOE (Molecular Operating Environment, 2022.02, Chemical Computing Group ULC, 1010 Sherbooke St. West, Suite #910, Montreal, QC, Canada, H3A2R7, 2023) structure preparation tools with default values. For producing the MD-starting structure the experimentally resolved residues of the Aβ were prolonged by either a serine or a phosphorylated serine in MOE.

The MD simulations were conducted using AMBER22 suite [93]. Topology and parameter files were generated in tleap module using the AMBER ff14sb. The simulations were set up in the following way: The peptide-aducanumab complex was energy minimized for 2000 steps using a generalized Born implicit solvent model, neutralized, and solvated using the TIP3P water model. The system was equilibrated by heating the solvent from 100 K to 300 K within 500 ps under constant volume conditions with non-solvent atoms assigned with harmonic constraints of 100 kcal·mol-1·Å-2. Cooling the system back to 100 K within 250 ps and lowering the harmonic constraints on non-solvent atoms to 1 kcal·mol-1·Å-2, followed by heating to 300 K within 500 ps period. Afterwards, the non-solvent atoms constraints were set off and the pressure was adjusted to 1 bar using the Berendsen barostat. Each complex (unmodified and phosphorylated) was simulated in triplicates for 200 ns at constant pressure and temperature. All simulations were carried out using periodic boundary and particle mesh

Ewald (PME) methodology to handle long-range electrostatics. 2 fs-time steps were used for integration and coordinates of were saved every 500 steps (1 ps). The trajectories were further analysed with CPPTRAJ (4.14.0).

Aβ-Peptides for SDS-PAGE, CIEF Immunoassay and IP-MS

The synthetic peptides Aβ1–40, Aβ1–42, Aβ2–40, Aβ3–40, AβpE3–40, Aβ4–40, Aβ5–40 and Aβ11–40 were obtained from AnaSpec (Fremont, California, USA 94555).~~whether Aβ1-16, Aβ1-34 and Aβ1-38 from StressMarq (Victoria, British Columbia, Canada)~~. Synthetic Aβ−3–40 [94]was kindly provided by H.-J. Knölker, Technische Universität Dresden. Phosphorylated pSer8-Aβ1-40 was synthesized with an amidated C-terminal carboxyl group to remove one negative charge, ensuring that this Aβ variant still falls into the applied separation range of the CIEF immunoassay.

Bistris-SDS Gradient PAGE/Western Blots Analysis of Different Aβ Aggregation States

For the assessment of antibody binding to different Aβ aggregation states, we used Aβ1-42 monomers (Cat. No SPR-485B), Aβ1-42 oligomers (Cat. No SPR-488B) and preformed Aβ1-42 fibrils (Cat. No SPR-487B) (StressMarq biosciences, Victoria, BC, Canada). The samples for electrophoresis were prepared (starting from stock solutions) with final concentrations of 0.1 µg/µL) in LDS sample buffer (247.5 mM Tris-HCl, pH 8.5, 2% (w/v) lithium dodecyl sulfate (LDS), 10% (v/v) glycerol, 0.5 mM EDTA, 0.22 mM Brilliant Blue G250, 0.175 mM Phenol Red) and denatured by heating at 70°C for 10 min. Per lane, 0.361, 0.722 or 1.44 µg of the different Aβ1-42 forms were loaded on a 4-12% Bistris-gel (1mm, 12 wells, Anamed Electrophorese GmbH, Groß-Bieberau / Rodau, Germany) and separated at 200 V using MES-SDS running buffer. Following recommendations provided by the manufacturer of the different Aβ1-42 aggregation forms, electroblotting onto nitrocellulose was done at 100 V for 1 hour with a Biorad mini tank blot. The prechilled transfer buffer contained 25 mM Tris, 192 mM glycine, 20% (v/v) methanol and 0.0375 % Tween-20. After blotting, the membrane was washed for 10 min at room temperature in Tris-buffered saline (TBS) followed by blocking for 30 min with 5% powdered milk in TBS containing 0.1% Tween-20 (TBS-T). The blots were then incubated with primary antibodies in 5% milk in TBS-T over night at 4°C and washed 3 x for 10 min with TBS-T at room temperature. The secondary antibodies were (i) Peroxidase-conjugated Affini Pure Donkey Anti-Human IgG (H+L), Jackons ImmunoResearch

900 Laboratories Inc., West Grove, PA, (code number 709-035-149)1:20000 in TBS-T for
901 Donanemab$_{bs}$, Lecanemab$_{bs}$ and Aducanumab$_{bs}$ and (ii) anti-mouse IgG-POD
902 (Calbiochem/EMD Millipore, San Diego, California, USA, catalog number 401253-2ML)
903 1:10000 in TBS-T for mAb 1E4E11 and mAb 6E10. After 1 h incubation with the secondary
904 antibodies, the blots were washed 3 x for 10 min with TBS-T and incubated for 5 min with
905 ECL-Prime Western Blotting Detection Reagent (Cytiva Amersham, Little Chalfont, England).
906 Images were recorded on a Vilber-Loumart Fusion SL blot imager. To confirm successful
907 blotting of all Aβ variants, the blot membranes were reprobed without prior stripping with
908 mAb4G8 (0.5 µg/mL in 5% milk in TBS-T over night at 4°C or 1-2 h at room temperature)
909 followed by anti-mouse IgG-POD (1:10000 in TBS-T) for 1 h at room temperature. That way,
910 the 4G8 reprobing signals were essentially added on top of the initial signals and background
911 artifacts.

912 Peptide Bicine-Tris SDS-PAGE / Western Blot

913 Synthetic Aβ peptides were separated by 15% T/5% C Bicine-Tris SDS-PAGE, essentially
914 according to[95]. After the electrophoresis, the gel was shortly rinsed with 50 mM Tris –HCl,
915 pH 8.0, followed by blotting the peptides on PVDF using a Gravity Blotter (Serva
916 Electrophoresis GmbH, Heidelberg, Germany). The blotting sandwich was assembled on the
917 Gravity blotter from bottom to top by first placing the gel on the lower plate, followed by a
918 precut PVDF membrane (activated with methanol and equilibrated in 50 mM Tris-HCl, pH
919 8.0), one filter paper Whatmann 3mM equilibrated in 50 mM Tris-HCl, pH 8.0, three dry filter
920 papers (Sartorius BF4 blotting paper) and, finally, three 2.25 kg Gravity Blotter metal plates.
921 The gravity/press blotting was done overnight at room temperature. On the next morning, the
922 blot sandwich was disassembled and the PVDF membrane was boiled in PBS for 3min in a
923 microwave oven with the protein side facing downwards. After blocking for 30 min at room
924 temperature with 2% ECL Prime blocking reagent (Cytiva) in PBS containing 0.075% Tween-
925 20 (PBS-T), the blots were incubated for 1 h at room temperature with the primary antibodies
926 (0.5 µg/mL in 2% ECL-Prime Western Blotting Detection Reagent in PBS-T). After 3 x 10
927 min washing with PBS-T, the secondary peroxidase-conjugated Affini Pure Donkey Anti-
928 Human IgG (see above) (1:20000 in PBS-T) was applied for 1-2 hours at room temperature.
929 Following 3 x 10 min washing with PBS-T, the blots were incubated for 5 min with ECL-Prime
930 Western Blot Detection Reagent, and images were recorded. To confirm successful blotting of
931 all Aβ variants, the blot membranes were reprobed without prior stripping with mAb4G8 (0.5

932 µg/mL in 2% ECL Prime blocking reagent in PBS-T over night at 4° C or 1 h at room
933 temperature followed by anti-mouse IgG-POD (1:10000 in PBS-T) for 1 h at room temperature.
934 That way, the 4G8 reprobing signals were essentially added on top of the initial signals and
935 background artifacts.

936 Capillary Isoelectric Focusing Immunoassay

937 Automated capillary isoelectric focusing immunoassays were performed with a Peggy-Sue
938 system (ProteinSimple,San Jose, California, USA), essentially as previously described [96] and
939 [53].

940 In brief, synthetic Aβ peptide variants were separated by isoelectric focusing in
941 microcapillaries followed by photochemical immobilization to the inner capillary walls and
942 probing with the primary antibodies for 120 min. After 2 washes, the horseradish peroxidase
943 conjugated secondary antibodies were loaded and incubated for 60 min. After two washing
944 steps, a luminol/peroxide mix was loaded, and chemiluminescent signals were recorded. The
945 data was analyzed with the Compass for SW software. The following secondary antibodies
946 were used: Anti-human IgG Secondary HRP antibody (Protein Simple, catalog number 043-
947 491), Goat-Anti-Mouse-HRP Secondary Antibody ProteinSimple, catalog number 040-655)
948 and Peroxidase-conjugated Affini Pure Donkey Anti-Human IgG (H+L) (1:100 dilution)
949 (Jackson ImmunoResearch Laboratories Inc., West Grove, PA, code number 709-035-149).

950 Automated Solid Phase Peptide Synthesis

951 The peptides were synthesized using PurePep Chorus (Gyros Protein Technologies, US) with
952 Fmoc chemistry at 0.05mmol scale. Tentagel S RAM (Resin Substitution 0.22mmol/g - Rapp
953 Polymere, Germany) resin was first swollen in dimethylformamide (DMF) for 30-60 minutes.
954 Next, Fmoc was removed using a 20% piperidine in DMF solution for 1-2 minutes and washed
955 3x with DMF. Deprotection steps were performed at 90°C for unphosphorylated peptides and
956 at room temperature from the first phospho-serine coupling. The peptide chain was elongated
957 by adding the premixed amino acid (AA, 125mM and Oxyma 125mM) along with N,N'-
958 diisopropylcarbodiimide (DIC, 250mM). The mixture was heated at 90°C for 2 minutes and
959 then washed 2x with DMF. Capping was done with acetic anhydride (10% in DMF) for 5
960 minutes and washed 3x with DMF. The peptide chain was elongated until completion and dried
961 for 30 minutes after 7x DCM washes. The Fmoc deprotected peptides were cleaved from the

962 resin using a mixture of 90% TFA, 5% water, 3% TIPS, and 2% DCM for 4 h at RT. The
963 peptides were then precipitated in ice-cold ether ON, subsequently purified using HPLC and
964 analysed by LC-MS, as described below.

965 Purification and Characterization of Peptides

966 The crude peptides were purified by reverse phase (RP) HPLC using a water-acetonitrile
967 gradient with 0.1% formic acid (FA). Preparative HPLC was performed on a UltiMate™ 3000
968 HPLC Systems instrument (ThermoFisher Scientific, Waltham, Massachusetts, USA)
969 equipped with RS variable wavelength detector (set to 215nm) and a Kinetex® 5µm EVO C18
970 100 LC column (00D-4633-P0-AX; Phenomenex, Aschaffenburg, Germany). Chromatograms
971 were recorded using Chromeleon software v7.2. Purity and structural identity of the peptides
972 were verified using a DAD equipped 1260 Infinity II HPLC device with a C18 RP column
973 (Onyx Monolithic C18 50×2 mm), coupled to a mass selective detector with a single
974 quadrupole system (Agilent Technologies, Santa Clara, CA, US) in ESI+ mode.

975 Crude phosphorylated pSer8-Aβ1-40 with an amidated C-terminal carboxyl group was purified
976 on a 10x150mm Waters (Milford, Massachusetts, USA) XBridge Protein BEH C4 OBD
977 preparative column (300Å, 5 µm) using 3% acetonitrile/0.2% Formic acid as solvent A and
978 97% acetonitrile/0.2% FA as solvent B. A Beckman System Gold HPLC system with external
979 column oven was used to form the following gradient with a flow rate of 3.8 ml/min at 50°C
980 column temperature: 5-20% B in 2 min, 20-32% B in 22 min, 32-50% in 5 min. Analytical
981 HPLC was performed on a Waters Alliance e2695 HPLC system coupled to a photodiode array
982 (PDA) optic detector and a single quadrupole QDa mass detector. A 4.6x150mm Waters
983 XBridge Protein BEH C4 analytical column (300 Å, 3.5µm) was used at a flow rate of
984 3.8ml/min at 50°C column temperature; the corresponding gradient was 5-20% B in 2 min, 20-
985 32% B in 11 min, 32-50% in 5 min.

986 Biolayer Interferometry

987 The samples were dispensed into a 96 microplate (Greiner bio-one GmbH, Frickenhausen,
988 Germany) at a final volume of 200 µL. The binding of Aducanumab biosimilar and mAb
989 1E4E11 and their phosphorylated, unphosphorylated and H6R epitopes 6xHis-tagged were
990 measured using Biolayer interferometry on an Octet RED 96system (Sartorius, Göttingen,
991 Germany). The peptides were synthesized (purity above 98% - based on UV at 215nm) with

992 Fmoc-Adoa linker (Iris - FAA1435) and C-terminal 6xHis tag. Sensorgrams were measured in
993 double reference against the buffer and the reference sensor signals.

994 NTA biosensors (Sartorius, Göttingen, Germany) were preincubated into 1XPBS buffer pH
995 7.4, 0.2% BSA, 0.02% (v/v) Tween 20 for 10 min. A first baseline was established in the same
996 buffer. The 6xHis peptides were loaded onto NTA biosensors at 20 µg/ml for 200 s. Following
997 a buffer wash of 120s, the biosensors were incubated with serial-dilutions of the respective
998 antibodies for 1200s s to measure association and then into buffer for additional 1500s to
999 observe the dissociation phase. Experiments were performed at 30℃ and sample plates were
1000 shaken at 1000 rpm. Sensorgrams were globally fitted using Data Analysis software version
1001 12.0.2.3 (Sartorius, Göttingen, Germany) with a 1:1 binding model.

1002 Immunoprecipitation and Mass Spectrometry

1003 Antibodies were covalently coupled to Dynabeads M-270 Epoxy (Invitrogen/ThermoFisher
1004 Scientific, Waltham, Massachusetts, USA Cat. No. 14311 D), essentially following the
1005 manufacturer's instructions. Tween-20 was omitted from all wash and storage buffers for
1006 specific use in IP-MS. In brief, 5 mg of M-270 epoxy beads were weighed into a 1.5-mL
1007 reaction vial and washed with 1 mL of buffer C1 (kit component). The bead suspension was
1008 divided in aliquots of 200 µL (containing 1mg of beads). The vials were placed on a magnetic
1009 stand for a few minutes, and the supernatant was carefully removed and discarded. Washed
1010 beads were resuspended in 40 µL of buffer C1 and 10 µL of antibody stock solution (1 mg/mL).
1011 After gentle mixing by pipetting, 50 µL of buffer C2 (kit component) was added and incubated
1012 overnight at 37 °C on a mixer. After coupling, the beads were washed one time with 400 µL of
1013 buffer HB (kit component), one time with 400 µL of buffer LB (kit component) and two times
1014 with 400 µL of PBS. After a final wash with PBS for 15 min with continuous agitation, the
1015 beads were resuspended in 100 µL PBS/0.1% BSA/0.02% NaN_3 and stored at 4 °C.

1016 The synthetic Aβ peptides Aβ1–40, pSer8-Aβ1–40, Aβ1–42, Aβ2–40, Aβ3–40, AβpyGlu–40,
1017 Aβ4–40, Aβ5–40 and Aβ11–40 Aβ−3–40 (see above), were mixed and diluted to final
1018 concentrations of 10ng/mL of each in PBS/0.1%BSA containing phosphatase inhibitors
1019 (PhosphoStop Mini, Roche, Ref 04906837001) and protease inhibitors (Complete Mini Roche,
1020 Ref 04693124001). For immunoprecipitation of Aβ peptides, 250 µL of the Aβ mix or of
1021 pooled CSF was combined with an equal volume of 100 mM Tris-HCl, pH 7.4, containing
1022 0.2% (w/v) nonyl-β-d-thiomaltoside (NTM) and 0.2% (w/v) n-dodecyl-β-d-maltoside (DDM)

1023 and 15 µL of functionalized M270 epoxy beads. After overnight incubation at 4 °C with
1024 constant mixing, the beads were washed five times with 0.5 mL of 50 mM Tris-HCl, pH 7.4,
1025 150 mM NaCl, 0.1% (w/v) DDM, 0.1% (w/v) NTM and resuspended in 0.5 mL of 50 mM
1026 ammonium acetate (pH approximately 7.0). The beads were immediately forwarded to sample
1027 preparation for mass spectrometry. There, the beads were immobilised on a magnet, the
1028 supernatant was removed, and the beads were washed one time with 0.5 mL of 50 mM
1029 ammonium acetate, and one time with 0.5 mL H_2O. The bound Aβ peptides were eluted in 2.5
1030 µL of 70% acetonitrile containing 5 mM HCl.

1031 Analysis by MALDI-TOF-MS was essentially performed as described [21,97]. Briefly, the
1032 eluates (0.5 µL) from synthetic samples were spotted onto a pre-structured MALDI sample
1033 support (MTP AnchorChip 384 BC; Cat. No. 8280790, Bruker, Bremen, Germany), followed
1034 by the addition of 0.5 µl TOPAC matrix solution, a matrix recently developed for the improved
1035 detection of intact phosphorylated Aβ peptides [82]. Alternatively, conventional CHCA matrix
1036 was used for CSF samples as described in [21]. A 1:1 mixture of Peptide Calibration Standard
1037 II (Cat. No. 8222570, Bruker, Bremen, Germany) and PepMix2 (Cat. No. C102, LaserBio
1038 Labs, Valbonne, France) was used as calibrant. The samples were dried in a vacuum desiccator
1039 and a total of 5000 mass spectra per spot were recorded using an ultrafleXtreme MALDI-
1040 TOF/TOF mass spectrometer in reflector mode operated under the software flexControl 3.4
1041 (Bruker, Bremen, Germany).

1042 Immunohistochemistry and Antibody Preadsorption

1043 Immunohistochemistry was performed on 4-µm paraffin sections. In brief, brain sections were
1044 deparaffinized in Roticlear (Carl Roth, Karlsruhe, Germany) and rehydrated in a descending
1045 series of ethanol. Activity of endogenous peroxidases was blocked by incubation in 0.3% H_2O_2
1046 in PBS for 30 min. Antigen retrieval was achieved by initial boiling of the sections in 0.01 M
1047 citrate buffer (pH 6.0) and subsequent incubation in 88% formic acid for 3 min. Unspecific
1048 binding sites were blocked by incubation in PBS containing 4% skim milk and 10% fetal calf
1049 serum (FCS) for 1 h at room temperature, prior to the overnight incubation with the primary
1050 antibodies. The following antibodies were used for the detection of different Aβ variants:
1051 $Aducanumab_{bs}$ (0.5 µg/µl), $Donanemab_{bs}$ (1 µg/ml), $Lecanemab_{bs}$ (0.06 µg/ml).

1052 Antibody pre-adsorption with synthetic Aβ peptides (Aβ1-16 (synthesized at Neuroproteomics
1053 Group, Max-Planck Institute for Multidisciplary Sciences (MPI-NAT), Göttingen), Aβ1-34,

1054 Aβ1-38, Aβ1-40, Aβ3-40 (from Anaspec), AβpE-40 (Peptide Speciality Laboratory,
1055 Heidelberg, Germany), Aβ1-42 monomers, Aβ1-42 oligomers and Aβ1-42 fibrils (StressMarq,
1056 Victoria, Canada) was carried out as described previously [52]. In brief, 1 µg $Donanemab_{bs}$
1057 was blocked with 2.5 µg of Aβ1-40, Aβ3-40 or AβpE3-40 in 0.01 M PBS including 10% FCS.
1058 In the case of $Aducanumab_{bs}$, 0.5 µg of the antibody were blocked with 10 µg of Aβ1-42
1059 monomers or 5 µg of Aβ1-42 fibrils. For $Lecanemab_{bs}$, 0.06 µg of antibody (PX-TA1746) was
1060 blocked with 0.25 µg of Aβ1-42 monomers, oligomers or fibrils, or 0.06 µg (BXC-SIM0032)
1061 was blocked with 0.25 µg Aβ1-16, Aβ1-34, Aβ1-38 or Aβ1-42 monomers). Antibodies and
1062 peptides were incubated on a rotator for 3 h at room temperature and reaction tubes were
1063 centrifuged at 13000 rpm for 5 min at the end of the incubation period. Control conditions
1064 included antibodies in 0.01 M PBS including 10% FCS without synthetic peptides. Adjacent
1065 paraffin-embedded sections from a human AD case were incubated overnight with the
1066 supernatants and sections were washed with 0.01 M PBS including 0.1 % Tergitol. For
1067 detection, biotinylated anti-human antibodies (6 µg/ml, Jackson ImmunoResearch, West
1068 Grove, Pennsylvania, USA #109-065-003) were used and staining was visualized with the
1069 ABC method with a Vectastain kit (Vector Laboratories, Newark, California, USA),
1070 diaminobenzidine as a chromogen and counterstaining with hematoxylin.

1071 Author contributions

1072 The following section was based on the CRediT system. Conceptualization: IT, HMM;
1073 Methodology: IT, HMM, HWK, OJ, OW; Formal Analysis: IT, HMM, TLe, HWK, OJ, OW,
1074 SB, LvW, TLi; Investigation: IT, TLe, HWK, MMH, SA, BM, SB, LvW, TLi; Visualization:
1075 IT, TLe; Writing – Original Draft: HMM, IT; Writing – review & editing: all the co-authors;
1076 Project administration: IT, HMM; Supervision: HMM, HWK, OJ, OW, JW, HS, JoW, JeW;
1077 Funding Acquisition, HMM.

1078 Acknowledgements

1079 First, we thank Sonja Kachler, Gabriele Paetzold and Sandra Theil for the excellent technical
1080 assistance. Also, we would like to thank Prof. S. Weggen (Heinrich Heine University,
1081 Germany) to have kindly provided the IC16 Antibody. We thank Prof. H.-J. Knölker
1082 (Technische Universität Dresden, Germany) for providing the synthetic Aβ-3-40 peptide. We
1083 thank Niels Hansen and Anke Jahn Brodmann for support and for providing CSF-samples from

the local biobank. H.M.M. acknowledge funding by the Interdisziplinäres Zentrum für Klinische Forschung (IZKF) of Würzburg, project number A-F-N-419. H.M.M. acknowledges the Junior Group Leader program of the Rudolf Virchow Center, the excellent ideas programme of the University of Würzburg and support through the Emmy Noether Programme of the Deutsche Forschungsgemeinschaft (DFG) (MA6957/1-1). T.L. acknowledges funding by the Graduate School of Life Sciences of the University of Würzburg. O.W. acknowledges funding by the DFG (WI3472/11-1 and Research Training Group 2824 (RTG2824)). J.W acknowledges funding by the DFG WA1477/6-6. M.M.H is a member of RTG 2824 funded by the DFG.

Competing interests

The authors declare that there are no competing interests related to this manuscript.

References

1. Colvin, M.T. *et al.* (2016) Atomic Resolution Structure of Monomorphic Aβ42 Amyloid Fibrils. *Journal of the American Chemical Society* 138, 9663-9674. 10.1021/jacs.6b05129
2. Yang, Y. *et al.* (2022) Cryo-EM structures of amyloid-β 42 filaments from human brains. *Science* 375, 167-172. doi:10.1126/science.abm7285
3. Tzioras, M. *et al.* (2023) Synaptic degeneration in Alzheimer disease. *Nature Reviews Neurology* 19, 19-38. 10.1038/s41582-022-00749-z
4. Kent, S.A. *et al.* (2020) The physiological roles of tau and Aβ: implications for Alzheimer's disease pathology and therapeutics. *Acta Neuropathologica* 140, 417-447. 10.1007/s00401-020-02196-w
5. Vassar, R. *et al.* (1999) β-Secretase Cleavage of Alzheimer's Amyloid Precursor Protein by the Transmembrane Aspartic Protease BACE. *Science* 286, 735-741. 10.1126/science.286.5440.735
6. Wolfe, M.S. *et al.* (1999) Two transmembrane aspartates in presenilin-1 required for presenilin endoproteolysis and γ-secretase activity. *Nature* 398, 513-517. 10.1038/19077
7. Wiltfang, J. *et al.* (2002) Highly conserved and disease-specific patterns of carboxyterminally truncated Aβ peptides 1–37/38/39 in addition to 1–40/42 in Alzheimer's disease and in patients with chronic neuroinflammation. *Journal of Neurochemistry* 81, 481-496. https://doi.org/10.1046/j.1471-4159.2002.00818.x
8. Mukherjee, S. *et al.* (2021) Citrullination of Amyloid-β Peptides in Alzheimer's Disease. *ACS Chemical Neuroscience* 12, 3719-3732. 10.1021/acschemneuro.1c00474
9. Scheidt, H.A. *et al.* (2020) Structural characteristics of oligomers formed by pyroglutamate-modified amyloid β peptides studied by solid-state NMR. *Physical Chemistry Chemical Physics* 22, 16887-16895. 10.1039/D0CP02307H

10. Grochowska, K.M. *et al.* (2017) Posttranslational modification impact on the mechanism by which amyloid-β induces synaptic dysfunction. *EMBO reports* 18, 962-981. https://doi.org/10.15252/embr.201643519
11. Roher, A.E. *et al.* (1993) Structural alterations in the peptide backbone of beta-amyloid core protein may account for its deposition and stability in Alzheimer's disease. *Journal of Biological Chemistry* 268, 3072-3083. https://doi.org/10.1016/S0021-9258(18)53661-9
12. Moro, M.L. *et al.* (2018) Pyroglutamate and Isoaspartate modified Amyloid-Beta in ageing and Alzheimer's disease. *Acta Neuropathologica Communications* 6, 3. 10.1186/s40478-017-0505-x
13. Schrempel, S. *et al.* (2024) Identification of isoAsp7-Aβ as a major Aβ variant in Alzheimer's disease, dementia with Lewy bodies and vascular dementia. *Acta Neuropathologica* 148, 78. 10.1007/s00401-024-02824-9
14. Kumar, S. *et al.* (2021) Novel Phosphorylation-State Specific Antibodies Reveal Differential Deposition of Ser26 Phosphorylated Aβ Species in a Mouse Model of Alzheimer's Disease. *Frontiers in Molecular Neuroscience* 13. 10.3389/fnmol.2020.619639
15. Ashby, E.L. *et al.* (2015) Investigation of Aβ phosphorylated at serine 8 (pAβ) in Alzheimer's disease, dementia with Lewy bodies and vascular dementia. *Neuropathology and Applied Neurobiology* 41, 428-444. https://doi.org/10.1111/nan.12212
16. Kumar, S. *et al.* (2012) Phosphorylation of Amyloid-β Peptide at Serine 8 Attenuates Its Clearance via Insulin-degrading and Angiotensin-converting Enzymes*. *Journal of Biological Chemistry* 287, 8641-8651. https://doi.org/10.1074/jbc.M111.279133
17. Wirths, O. and Zampar, S. (2019) Emerging roles of N- and C-terminally truncated Aβ species in Alzheimer's disease. *Expert Opinion on Therapeutic Targets* 23, 991-1004. 10.1080/14728222.2019.1702972
18. Shinohara, M. *et al.* (2017) Distinct spatiotemporal accumulation of N-truncated and full-length amyloid-β42 in Alzheimer's disease. *Brain* 140, 3301-3316. 10.1093/brain/awx284
19. Reinert, J. *et al.* (2016) Deposition of C-terminally truncated Aβ species Aβ37 and Aβ39 in Alzheimer's disease and transgenic mouse models. *Acta Neuropathologica Communications* 4, 24. 10.1186/s40478-016-0294-7
20. Moro, M.L. *et al.* (2012) APP mutations in the Aβ coding region are associated with abundant cerebral deposition of Aβ38. *Acta Neuropathologica* 124, 809-821. 10.1007/s00401-012-1061-x
21. Wirths, O. *et al.* (2024) Amino-terminally elongated Aβ peptides are generated by the secreted metalloprotease ADAMTS4 and deposit in a subset of Alzheimer's disease brains. *Neuropathology and Applied Neurobiology* 50, e12991. https://doi.org/10.1111/nan.12991
22. Sinha, S. *et al.* (1999) Purification and cloning of amyloid precursor protein β-secretase from human brain. *Nature* 402, 537-540. 10.1038/990114
23. Walter, S. *et al.* (2019) The metalloprotease ADAMTS4 generates N-truncated Aβ4–x species and marks oligodendrocytes as a source of amyloidogenic peptides in Alzheimer's disease. *Acta Neuropathologica* 137, 239-257. 10.1007/s00401-018-1929-5
24. Wirths, O. *et al.* (2017) N-truncated Aβ4–x peptides in sporadic Alzheimer's disease cases and transgenic Alzheimer mouse models. *Alzheimer's Research & Therapy* 9, 80. 10.1186/s13195-017-0309-z

25. Seuma, M. *et al.* (2021) The genetic landscape for amyloid beta fibril nucleation accurately discriminates familial Alzheimer's disease mutations. *eLife* 10, e63364. 10.7554/eLife.63364
26. Paravastu, A.K. *et al.* (2008) Molecular structural basis for polymorphism in Alzheimer's amyloid fibrils. *Proceedings of the National Academy of Sciences* 105, 18349-18354. doi:10.1073/pnas.0806270105
27. Tycko, R. (2015) Amyloid Polymorphism: Structural Basis and Neurobiological Relevance. *Neuron* 86, 632-645. https://doi.org/10.1016/j.neuron.2015.03.017
28. Qiang, W. *et al.* (2017) Structural variation in amyloid-β fibrils from Alzheimer's disease clinical subtypes. *Nature* 541, 217-221. 10.1038/nature20814
29. Lu, J.-X. *et al.* (2013) Molecular Structure of β-Amyloid Fibrils in Alzheimer's Disease Brain Tissue. *Cell* 154, 1257-1268. https://doi.org/10.1016/j.cell.2013.08.035
30. Rasmussen, J. *et al.* (2017) Amyloid polymorphisms constitute distinct clouds of conformational variants in different etiological subtypes of Alzheimer's disease. *Proceedings of the National Academy of Sciences* 114, 13018-13023. doi:10.1073/pnas.1713215114
31. Barykin, E.P. *et al.* (2017) Amyloid β Modification: A Key to the Sporadic Alzheimer's Disease? *Frontiers in Genetics* 8. 10.3389/fgene.2017.00058
32. Kummer, M.P. and Heneka, M.T. (2014) Truncated and modified amyloid-beta species. *Alzheimer's Research & Therapy* 6, 28. 10.1186/alzrt258
33. Roher, A.E. *et al.* (2017) APP/Aβ structural diversity and Alzheimer's disease pathogenesis. *Neurochemistry International* 110, 1-13. https://doi.org/10.1016/j.neuint.2017.08.007
34. Gómez-Castro, C.Z. *et al.* (2024) An N-terminal acidic β-sheet domain is responsible for the metal-accumulation properties of amyloid-β protofibrils: a molecular dynamics study. *JBIC Journal of Biological Inorganic Chemistry*. 10.1007/s00775-024-02061-1
35. Gessel, M.M. *et al.* (2012) Familial Alzheimer's Disease Mutations Differentially Alter Amyloid β-Protein Oligomerization. *ACS Chemical Neuroscience* 3, 909-918. 10.1021/cn300050d
36. Hatami, A. *et al.* (2017) Familial Alzheimer's Disease Mutations within the Amyloid Precursor Protein Alter the Aggregation and Conformation of the Amyloid-β Peptide* *This work was supported by National Institutes of Health Grants AG033069 and AG00538 and a grant from the Cure Alzheimer's fund. The authors declare that they have no conflicts of interest with the contents of this article. The content is solely the responsibility of the authors and does not necessarily represent the official views of the National Institutes of Health. *Journal of Biological Chemistry* 292, 3172-3185. https://doi.org/10.1074/jbc.M116.755264
37. Jang, H. *et al.* (2013) Familial Alzheimer's Disease Osaka Mutant (ΔE22) β-Barrels Suggest an Explanation for the Different Aβ1–40/42 Preferred Conformational States Observed by Experiment. *The Journal of Physical Chemistry B* 117, 11518-11529. 10.1021/jp405389n
38. Söderberg, L. *et al.* (2024) Amyloid-beta antibody binding to cerebral amyloid angiopathy fibrils and risk for amyloid-related imaging abnormalities. *Scientific Reports* 14, 10868. 10.1038/s41598-024-61691-2
39. van Dyck, C.H. (2018) Anti-Amyloid-β Monoclonal Antibodies for Alzheimer's Disease: Pitfalls and Promise. *Biological Psychiatry* 83, 311-319. https://doi.org/10.1016/j.biopsych.2017.08.010
40. Sevigny, J. *et al.* (2016) The antibody aducanumab reduces Aβ plaques in Alzheimer's disease. *Nature* 537, 50-56. 10.1038/nature19323

41. Arndt, J.W. *et al.* (2018) Structural and kinetic basis for the selectivity of aducanumab for aggregated forms of amyloid-β. *Scientific Reports* 8, 6412. 10.1038/s41598-018-24501-0
42. Feinberg, H. *et al.* (2014) Crystal structure reveals conservation of amyloid-β conformation recognized by 3D6 following humanization to bapineuzumab. *Alzheimer's Research & Therapy* 6, 31. 10.1186/alzrt261
43. Budd Haeberlein, S. *et al.* (2022) Two Randomized Phase 3 Studies of Aducanumab in Early Alzheimer's Disease. *J Prev Alzheimers Dis* 9, 197-210. 10.14283/jpad.2022.30
44. Dyer, O. (2024) Aduhelm: Biogen abandons Alzheimer's drug after controversial approval left it unfunded by Medicare. *BMJ* 384, q281. 10.1136/bmj.q281
45. Honig, L.S. *et al.* (2024) Updated safety results from phase 3 lecanemab study in early Alzheimer's disease. *Alzheimers Res Ther* 16, 105. 10.1186/s13195-024-01441-8
46. Peralta Reyes, F.S. *et al.* (2025) Lecanemab Binds to Transgenic Mouse Model-Derived Amyloid-beta Fibril Structures Resembling Alzheimer's Disease Type I, Type II and Arctic Folds. *Neuropathol Appl Neurobiol* 51, e70022. 10.1111/nan.70022
47. Sims, J.R. *et al.* (2023) Donanemab in Early Symptomatic Alzheimer Disease. *JAMA* 330, 512-527. 10.1001/jama.2023.13239
48. Dyck, C.H.v. *et al.* (2023) Lecanemab in Early Alzheimer's Disease. *New England Journal of Medicine* 388, 9-21. doi:10.1056/NEJMoa2212948
49. Mintun, M.A. *et al.* (2021) Donanemab in Early Alzheimer's Disease. *New England Journal of Medicine* 384, 1691-1704. doi:10.1056/NEJMoa2100708
50. Shcherbinin, S. *et al.* (2022) Association of Amyloid Reduction After Donanemab Treatment With Tau Pathology and Clinical Outcomes: The TRAILBLAZER-ALZ Randomized Clinical Trial. *JAMA Neurology* 79, 1015-1024. 10.1001/jamaneurol.2022.2793
51. Britschgi, M. *et al.* (2009) Neuroprotective natural antibodies to assemblies of amyloidogenic peptides decrease with normal aging and advancing Alzheimer's disease. *Proceedings of the National Academy of Sciences* 106, 12145-12150. doi:10.1073/pnas.0904866106
52. Klafki, H.-W. *et al.* (2022) Is plasma amyloid-β 1–42/1–40 a better biomarker for Alzheimer's disease than AβX–42/X–40? *Fluids and Barriers of the CNS* 19, 96. 10.1186/s12987-022-00390-4
53. Zampar, S. *et al.* (2020) N-terminal heterogeneity of parenchymal and vascular amyloid-β deposits in Alzheimer's disease. *Neuropathology and Applied Neurobiology* 46, 673-685. https://doi.org/10.1111/nan.12637
54. Savastano, A. *et al.* (2016) N-Truncated Aβ 2-X Starting with Position Two in Sporadic Alzheimer's Disease Cases and Two Alzheimer Mouse Models. *Journal of Alzheimer's Disease* 49, 101-110. 10.3233/JAD-150394
55. Baghallab, I. *et al.* (2018) Epitomic Characterization of the Specificity of the Anti-Amyloid Aβ Monoclonal Antibodies 6E10 and 4G8. *Journal of Alzheimer's Disease* 66, 1235-1244. 10.3233/JAD-180582
56. Bader, A.S. *et al.* (2023) Brain Region-Specific Differences in Amyloid-β Plaque Composition in 5XFAD Mice. *Life* 13, 1053
57. Kumar, S. *et al.* (2013) Early intraneuronal accumulation and increased aggregation of phosphorylated Abeta in a mouse model of Alzheimer's disease. *Acta Neuropathologica* 125, 699-709. 10.1007/s00401-013-1107-8
58. Nussbaum, J.M. *et al.* (2012) Prion-like behaviour and tau-dependent cytotoxicity of pyroglutamylated amyloid-β. *Nature* 485, 651-655. 10.1038/nature11060

59. Bayer, T.A. and Wirths, O. (2014) Focusing the amyloid cascade hypothesis on N-truncated Abeta peptides as drug targets against Alzheimer's disease. *Acta Neuropathologica* 127, 787-801. 10.1007/s00401-014-1287-x
60. Klafki, H.W. *et al.* (2020) Development and Technical Validation of an Immunoassay for the Detection of APP669–711 (Aβ−3–40) in Biological Samples. *International Journal of Molecular Sciences* 21, 6564
61. Richter, L. *et al.* (2010) Amyloid beta 42 peptide (Aβ42)-lowering compounds directly bind to Aβ and interfere with amyloid precursor protein (APP) transmembrane dimerization. *Proceedings of the National Academy of Sciences* 107, 14597-14602. doi:10.1073/pnas.1003026107
62. Dornieden, S. *et al.* (2013) Characterization of a Single-Chain Variable Fragment Recognizing a Linear Epitope of Aβ: A Biotechnical Tool for Studies on Alzheimer's Disease? *PLOS ONE* 8, e59820. 10.1371/journal.pone.0059820
63. Jäger, S. *et al.* (2009) α-secretase mediated conversion of the amyloid precursor protein derived membrane stub C99 to C83 limits Aβ generation. *Journal of Neurochemistry* 111, 1369-1382. https://doi.org/10.1111/j.1471-4159.2009.06420.x
64. DeMattos, Ronald B. *et al.* (2012) A Plaque-Specific Antibody Clears Existing β-amyloid Plaques in Alzheimer's Disease Mice. *Neuron* 76, 908-920. https://doi.org/10.1016/j.neuron.2012.10.029
65. Kaneko, N. *et al.* (2014) Novel plasma biomarker surrogating cerebral amyloid deposition. *Proceedings of the Japan Academy, Series B* 90, 353-364. 10.2183/pjab.90.353
66. Nakamura, A. *et al.* (2018) High performance plasma amyloid-β biomarkers for Alzheimer's disease. *Nature* 554, 249-254. 10.1038/nature25456
67. Van Cauwenberghe, C. *et al.* (2016) The genetic landscape of Alzheimer disease: clinical implications and perspectives. *Genetics in Medicine* 18, 421-430. 10.1038/gim.2015.117
68. Weggen, S. and Beher, D. (2012) Molecular consequences of amyloid precursor protein and presenilin mutations causing autosomal-dominant Alzheimer's disease. *Alzheimer's Research & Therapy* 4, 9. 10.1186/alzrt107
69. Chen, W.T. *et al.* (2012) Amyloid-beta (Aβ) D7H mutation increases oligomeric Aβ42 and alters properties of Aβ-zinc/copper assemblies. *PLoS One* 7, e35807. 10.1371/journal.pone.0035807
70. Wakutani, Y. *et al.* (2004) Novel amyloid precursor protein gene missense mutation (D678N) in probable familial Alzheimer's disease. *Journal of Neurology, Neurosurgery & Psychiatry* 75, 1039. 10.1136/jnnp.2003.010611
71. Janssen, J.C. *et al.* (2003) Early onset familial Alzheimer's disease. *Neurology* 60, 235-239. doi:10.1212/01.WNL.0000042088.22694.E3
72. Jones, C.T. *et al.* (1992) Mutation in codon 713 of the β amyloid precursor protein gene presenting with schizophrenia. *Nature Genetics* 1, 306-309. 10.1038/ng0792-306
73. Peacock, M.L. *et al.* (1993) Novel polymorphism in the A4 region of the amyloid precursor protein gene in a patient without Alzheimer's disease. *Neurology* 43, 1254-1254. doi:10.1212/WNL.43.6.1254
74. Jonsson, T. *et al.* (2012) A mutation in APP protects against Alzheimer's disease and age-related cognitive decline. *Nature* 488, 96-99. 10.1038/nature11283
75. Yi, Y. *et al.* (2020) An APP mutation family exhibiting white matter hyperintensities and cortical calcification in East China. *Neurological Sciences* 41, 2921-2928. 10.1007/s10072-020-04342-4

76. Jiang, B. *et al.* (2019) Mutation screening in Chinese patients with familial Alzheimer's disease by whole-exome sequencing. *Neurobiology of Aging* 76, 215.e215-215.e221. https://doi.org/10.1016/j.neurobiolaging.2018.11.024
77. Obici, L. *et al.* (2005) A novel AβPP mutation exclusively associated with cerebral amyloid angiopathy. *Annals of Neurology* 58, 639-644. https://doi.org/10.1002/ana.20571
78. Aggarwal, L. and Biswas, P. (2021) Hydration Thermodynamics of the N-Terminal FAD Mutants of Amyloid-β. *Journal of Chemical Information and Modeling* 61, 298-310. 10.1021/acs.jcim.0c01286
79. Murakami, K. *et al.* (2003) Neurotoxicity and Physicochemical Properties of Aβ Mutant Peptides from Cerebral Amyloid Angiopathy. *Journal of Biological Chemistry* 278, 46179-46187. https://doi.org/10.1074/jbc.M301874200
80. Schlenzig, D. *et al.* (2009) Pyroglutamate Formation Influences Solubility and Amyloidogenicity of Amyloid Peptides. *Biochemistry* 48, 7072-7078. 10.1021/bi900818a
81. Kumar, S. *et al.* (2011) Extracellular phosphorylation of the amyloid peptide promotes formation of toxic aggregates during the pathogenesis of Alzheimer's disease. *The EMBO Journal* 30, 2255-2265. https://doi.org/10.1038/emboj.2011.138
82. Liepold, T. *et al.* (2023) Matrix Development for the Detection of Phosphorylated Amyloid-β Peptides by MALDI-TOF-MS. *Journal of the American Society for Mass Spectrometry* 34, 505-512. 10.1021/jasms.2c00270
83. Soderberg, L. *et al.* (2023) Lecanemab, Aducanumab, and Gantenerumab - Binding Profiles to Different Forms of Amyloid-Beta Might Explain Efficacy and Side Effects in Clinical Trials for Alzheimer's Disease. *Neurotherapeutics* 20, 195-206. 10.1007/s13311-022-01308-6
84. Frost, C.V. and Zacharias, M. (2020) From monomer to fibril: Abeta-amyloid binding to Aducanumab antibody studied by molecular dynamics simulation. *Proteins: Structure, Function, and Bioinformatics* 88, 1592-1606. https://doi.org/10.1002/prot.25978
85. Watt, A.D. *et al.* (2013) Oligomers, fact or artefact? SDS-PAGE induces dimerization of β-amyloid in human brain samples. *Acta Neuropathologica* 125, 549-564. 10.1007/s00401-013-1083-z
86. Butler, P.M. *et al.* (2025) Anti-amyloid antibody equilibrium binding to Abeta aggregates from human Alzheimer disease brain. *bioRxiv*. 10.1101/2025.05.20.654902
87. Schulte, C. *et al.* (2021) Low-cost synthesis of peptide libraries and their use for binding studies via temperature-related intensity change. *STAR protocols* 2, 100605
88. Talucci, I. *et al.* (2024) Molecular dissection of an immunodominant epitope in Kv1.2-exclusive autoimmunity. *Frontiers in Immunology* 15. 10.3389/fimmu.2024.1329013
89. Dikmans, A. *et al.* (2006) SC2: A Novel Process for Manufacturing Multipurpose High-Density Chemical Microarrays. *QSAR & Combinatorial Science* 25, 1069-1080. https://doi.org/10.1002/qsar.200640130
90. Frank, R. (1992) Spot-synthesis: an easy technique for the positionally addressable, parallel chemical synthesis on a membrane support. *Tetrahedron* 48, 9217-9232. https://doi.org/10.1016/S0040-4020(01)85612-X
91. Talucci, I. and Maric, H.M. (2023) Peptide Microarrays for Studying Autoantibodies in Neurological Disease. In *Peptide Microarrays: Methods and Protocols* (Cretich, M. and Gori, A., eds), pp. 17-25, Springer US
92. Kreissner, K.O. *et al.* (2024) MARTin—an open-source platform for microarray analysis. *Frontiers in Bioinformatics* 4. 10.3389/fbinf.2024.1329062

93. Case, D.A. *et al.* (2023) AmberTools. *Journal of Chemical Information and Modeling* 63, 6183-6191. 10.1021/acs.jcim.3c01153
94. Beyer, I. *et al.* (2016) Solid-Phase Synthesis and Characterization of N-Terminally Elongated Aβ−3–-Peptides. *Chemistry – A European Journal* 22, 8685-8693. https://doi.org/10.1002/chem.201600892
95. Wiltfang, J. *et al.* (1991) A new multiphasic buffer system for sodium dodecyl sulfate-polyacrylamide gel electrophoresis of proteins and peptides with molecular masses 100 000–1000, and their detection with picomolar sensitivity. *ELECTROPHORESIS* 12, 352-366. https://doi.org/10.1002/elps.1150120507
96. Haußmann, U. *et al.* (2013) Analysis of Amino-Terminal Variants of Amyloid-β Peptides by Capillary Isoelectric Focusing Immunoassay. *Analytical Chemistry* 85, 8142-8149. 10.1021/ac401055y
97. Klafki, H.-W. *et al.* (2022) Detection and quantification of Aβ−3–40 (APP669-711) in cerebrospinal fluid. *Journal of Neurochemistry* 160, 578-589. https://doi.org/10.1111/jnc.15571